NASA Technical Memorandum 88192

NASA-TM-88192 19860008821

Aerodynamic Characteristics of an Air-Exchanger System for the 40- by 80-Foot Wind Tunnel at Ames Research Center

Vernon J. Rossow, Gene I. Schmidt, Larry A. Meyn, Kimberley R. Ortner, and Robert E. Holmes

January 1986

National Aeronautics and Space Administration

NASA Technical Memorandum 88192

Aerodynamic Characteristics of an Air-Exchanger System for the 40- by 80-Foot Wind Tunnel at Ames Research Center

Vernon J. Rossow,
Gene I. Schmidt,
Larry A. Meyn,
Kimberley R. Ortner,
Robert E. Holmes, Ames Research Center, Moffett Field, California

January 1986

National Aeronautics and
Space Administration

Ames Research Center
Moffett Field, California 94035

CONTENTS

SYMBOLS

U.S. Customary Units are used throughout this report because of their appropriateness for the subject matter presented. They can be readily converted to SI units by recalling the following equivalents: 1 ft = 0.3048 m; 1 ft^2 = 0.0929 m^2; 1 lb/ft^2 = 47.88 N/m^2; 1 hp = 746 W; 1 Btu = 1055 J; 1 knot = 0.514 m/sec; and 1°F = 9/5°C + 32.

a least squares parameter, $t_o T'_o$

A area

b least squares parameter, $-T'_o$

C_p coefficient of heat capacity of air at constant pressure

C_s average coefficient of heat capacity of wind-tunnel structure

H total head = $p + \frac{1}{2}\rho V^2$

H_e heat energy added to tunnel airstream by models and engines in test section

k average coefficient of heat conductivity of tunnel surface

K_D drag coefficients of tunnel components referred to test section conditions

$\dot{m}$ air-exchange rate, equal to mass of air exchanged per unit time divided by mass flowing through test section per unit time

N number of points in data set

p static pressure

P power applied to drive fans

P_o power applied to drive fans when no air exchange

q dynamic pressure = $\frac{1}{2}\rho V^2$

R correlation coefficient, see equation (8)

S effective area of tunnel surface for heat transfer

t time

T temperature

V velocity

W_a weight of air contained by wind-tunnel circuit

$\dot{W}_{ex}$ weight flow rate of air being exchanged

W_s effective weight of tunnel structure that absorbs heat

δ effective thickness of tunnel surface for heat transfer

ΔT_m $T_m - T_o$ = asymptotic or maximum temperature rise of tunnel for a given heat-input rate and air-exchange rate

ρ air density

Subscripts:

atm atmospheric

bs bird screen

c cooling cycle

exh exhaust

i initial value

max maximum

n north leg of tunnel

opt optimum

s south leg of tunnel

ts test section

w west leg of tunnel

SUMMARY

A 1/50-scale model of the 40- by 80-Foot Wind Tunnel at Ames Research Center was used to study various air-exchange configurations. System components were tested throughout a range of parameters, and approximate analytical relationships were derived to explain the observed characteristics. It was found that the efficiency of the air exchanger could be increased (1) by adding a shaped wall to smoothly turn the incoming air downstream, (2) by changing to a contoured door at the inlet to control the flow rate, and (3) by increasing the size of the exhaust opening. The static pressures inside the circuit then remain within the design limits at the higher tunnel speeds if the air-exchange rate is about 5% or more. Since the model is much smaller than the full-scale facility, it was not possible to completely duplicate the tunnel, and it will be necessary to measure such characteristics as flow rate and tunnel pressures during implementation of the remodeled facility. The aerodynamic loads estimated for the inlet door and for nearby walls are also presented.

INTRODUCTION

The drive system in closed-circuit wind tunnels not only must accelerate tunnel air up to operating velocities, but must also maintain steady-state operating conditions for extended periods of time. In installations that do not provide for an exchange of air between the wind tunnel and the atmosphere, the power applied to the drive system is eventually converted to heat which is absorbed by the tunnel air, walls, and structure. As the temperature of the walls and structure rises, more and more heat is transferred by conduction through the walls to the atmosphere. If provisions are not made to augment the removal of heat energy, the temperature of the tunnel airstream and structure may rise to an equilibrium temperature which is excessive.

The heat buildup can be limited, however, through the use of a special heat-exchanger system so that the tunnel can operate for a longer or even an indefinite period at an acceptable temperature. A variety of schemes have been proposed and some implemented for subsonic wind tunnels (e.g., ref. 1). The methods include heat conduction through the walls only, heat transfer through a radiator-type cooler (with or without water cooling), and the exchange of hot air inside the tunnel for cooler outside air. Implementation of these techniques can be carried out by a wide variety of structural arrangements. The method chosen depends on the energy level

of the test section, the desired duration of test time, the size of the facility, the energy input of the models, and other such factors.

The two wind tunnels that comprise the National Full-Scale Aerodynamics Complex (NFAC) at Ames Research Center--the 40- by 80-Foot and 80- by 120-Foot tunnels (figs. 1 and 2)--exchange air to control tunnel temperatures. The 80 × 120 tunnel is an open-circuit, or flow-through, tunnel in which none of the test-section airstream is recirculated. It therefore does not have a cooling problem because any heat energy imparted to the airstream is discarded with the exhaust. Special consideration must however be given to the design of the inlet and exhaust openings to avoid excessive losses and to condition the airstream for the flow quality desired in the test section (see refs. 2-13). (Also, Schmidt, G. I.; Van Aken, J. M.; and Parrish, C. L.: Test Facility and Experimental Techniques Developed for 1/50 Scale Studies of the Ames 40- by 80- /80- by 120-Foot Wind Tunnel Complex. NASA TM in preparation.)

The 40 × 80 tunnel part of the NFAC is a closed-circuit facility which is cooled by an air-exchange system. That is, although most of the air is recirculated, a certain fraction is removed at one location in the circuit and an equal fraction is then replaced with fresh air from the atmosphere at another location in the circuit. The most recent design of the air exchanger for the 40 × 80 tunnel consisted of two louvered air inlet windows in the low-pressure (i.e., below atmospheric pressure), or north, leg of the return circuit, and three screened windows for air exhaust openings in the high-pressure (i.e., above atmospheric pressure), or south, leg of the facility (figs. 1, 2). Although any flow-field disruptions caused by the exhaust openings were not apparent, the inlet configuration was found to cause unacceptable distortion of the airstream entering the fan drive system. The difficulty became apparent when tests were begun in 1982 which would lead to the implementation of the facility. As the tunnel airspeed was increased, the two inboard, or courtyard, fans approached a stalled condition prematurely. Flow visualization (smoke) subsequently identified the source of the problem as the low-energy cooling air which enters through the courtyard inlet (fig. 3). It appears that the inlet windows direct the cooling air across rather than along the tunnel airstream. As a consequence, the two incoming airflows form plumes as they enter the wind tunnel. The plumes have little or no component of velocity along the circuit and thus form stagnant regions downstream of each of the inlets. This low-energy air does mix slowly with the main part of the airstream. The air-exchange inlet on the north wall is sufficiently far upstream of the corner and fans to achieve complete mixing of the low-energy cooling air that comes in through the inlet on the north wall. Thus, the flow into drive fans Nos. 3 and 6 is not seriously affected by the air-exchange system. The courtyard inlet, however, is so close to the corner (courtyard end of vane set No. 2) and to fans Nos. 1 and 4 that a low-speed layer of flow persists (fig. 3) right up to the fan face. As a consequence, about one half of the faces of fans Nos. 1 and 4 must cope with low-energy cooling air introduced through the courtyard inlet.

The foregoing observations led to the conclusion that improved air-exchange inlets should be considered. This paper describes the results of the study

subsequently undertaken to gather the aerodynamic information needed to design a satisfactory air-exchange system and to evaluate its operational characteristics. Considerations that influence the design are described, and theoretical estimates are made of several performance parameters. The experimental program was carried out with a 1/50-scale model of the NFAC (fig. 4) configured in the 40 × 80 tunnel mode of operation (Schmidt, Van Aken, and Parrish, in preparation). Whenever possible, the data generated with the small-scale model are compared with those from the full-scale facility. This procedure has led to (1) general design guidelines for an air-exchange system for closed-circuit wind tunnels in general; and (2) specific recommendations for the 40 × 80 tunnel at Ames.

GENERAL CONSIDERATIONS

Before proceeding with the study of the individual aspects of the air exchanger, the overall characteristics are discussed to establish a common basis for the entire system as it is integrated into the 40 × 80 tunnel. It should be noted that the type of air exchanger to be used is a passive system wherein neither the inlet nor the exhaust is driven (i.e., neither pressurized nor pumped). A flow rate at both openings is then established by the sizes of the openings and by the pressure difference between the inside of the tunnel and the outside (which is, of course, atmospheric pressure). The pressure difference across an opening depends on its location in the circuit and on the amount of air being exchanged. For example, the pressure difference is greatest (i.e., farthest below atmospheric) in the circuit where the velocity is the greatest, which is in the test section. The pressure is highest (and can exceed atmospheric pressure slightly) where the cross section of the tunnel is largest and the velocity lowest, which occurs in the south leg of the facility (figs. 1, 2).

Depending on how the inlet and exhaust openings are contoured, the local total pressure H, rather than the local static pressure p, may govern the flow rate through an orifice. The total pressure varies around the entire circuit because of friction on the walls, because of losses across the various vane sets, and also because the fan drive raises the total pressure. Hence, the lowest total head in the circuit is just upstream of the fan drive and the highest is just downstream. Since it is desirable that the incoming air have a total head equal to if not greater than the local value, the best location for the inlet would be just upstream of the drive fans. Unfortunately, vane sets Nos. 3 and 5 would interfere with any inlet openings nearby to an extent that any such location is impractical. The next most desirable location is just upstream of vane set No. 2 in the north leg of the circuit, which is where the old louvered inlets were placed. Measurements made during the 1982 tests indicate that the total pressure head H at that station in the center of the tunnel is about equal to or slightly less than atmospheric. Hence, if outside air is brought into the tunnel efficiently, the cooling air and the tunnel airstream should have nearly equal total heads. Since the static pressures will also be the same, the velocity of the incoming air should be about equal to the centerline value. Injection of cooling air could then be made to benefit the

velocity distribution in the north leg and into the fans by boosting the wall velocities to a value more nearly equal to the centerline value.

If the velocity distribution downstream of the inlet and of vane set No. 2 were also orderly, the cool air would remain distinct from the hot inside air and take on heat only as it cycles around the circuit until it finally spirals outward and leaves through the exhaust opening. It was found, however, from the 1/50-scale model that considerable mixing occurs downstream of the drive section because of the residual swirl from the six fans. The magnitude of the original temperature difference is then reduced by redistribution and mixing of the cool air with the hot air. The air leaving through the exhaust openings is then a mixture which has a temperature near the average for the tunnel. Location of the inlet and exhaust ports need then not be based specifically on the path of the cooling air but can be based on other factors such as structural convenience and efficiency. This permits the inlet location to be chosen where it will improve the circuit velocity profile the most. A downstream-facing scoop on either the courtyard or the north wall or on both of the north leg of the circuit was chosen for study. Such an inlet geometry (fig. 1), directs the in-drafted atmospheric air as an organized layer flowing in the direction of the primary flow of the wind tunnel (i.e., a wall jet) so that the energy level of the flow closest to the wall is effectively increased by the air intake system, thereby reducing the liklihood of fan stall. Since ceiling and floor locations are structurally impractical, they were not tested.

The exhaust openings are located at the west end of the south wall of the facility (fig. 2). The low magnitude of the velocity in the south leg suggests that a scoop-type removal contour would complicate the configuration substantially without much benefit over the use of simple door openings in vane set No. 7. It remains to be seen whether the lack of streamlined surfaces on the exhaust causes intolerable disturbances or not. Interference between vane set No. 6, the corner, and the exhaust opening (fig. 5), will also need to be studied.

Naturally, the size of the inlet and exhaust openings governs both the overall pressure level in the tunnel circuit and the air-exchange rate. The present investigation determined these relationships. It is necessary, however, to specify the requirements of the facility that are directly related to the air-exchange rate needed to maintain tolerable operating conditions. Since the tunnel heats as power is applied, the time available for test purposes without air exchange is limited by the heat capacity of (and conduction through) the structure, by the heat capacity of the air in the circuit, and by the maximum allowable temperature. Based on material properties of wire insulation, plastics, etc. used to assemble models, the maximum allowable temperature was set at 130°F. An estimate of the test time available on this basis with and without air exchange will be made in the next section of this paper. Adequacy of test time availability is then determined by comparison with the time needed to accomplish certain test or data objectives with a model in the test section. The time needed depends, of course, on the complexity of the model, on the changes made during a data run, and on the data reduction to be carried out on line before proceeding to the next data point. Typical test scenarios are presented in table 1 for two different types of models. These considerations suggest that 30 min

or more should be available on a continuous basis if research or developmental tests are to be conducted in a reasonably expeditious manner. The shutdown of a model and the reduction of power to cool down the tunnel from its maximum temperature are so disruptive and time consuming that certain minimum values of air-exchange rates need to be established to maintain the tunnel temperature below the 130°F limit so that a reasonable level of usefulness of the tunnel can be achieved. The energy-balance analysis presented in the next section develops equations with empirical constants to provide estimates of running times, temperature changes, and how they are affected by such items as air-exchange rate and powered models.

ANALYSIS OF RELATIONSHIP BETWEEN TUNNEL TEMPERATURE, AIR-EXCHANGE RATE, AND TIME

Problem Definition

The objective of the analysis presented here is to find equations with empirical constants that relate the air temperature in the tunnel to the air-exchange rate and the heat introduced by the drive fan motors and any heat added to the airstream by engines or by other heat sources in a model. (The present analysis is similar to an unpublished analysis carried out in 1974 by Kenneth W. Mort, Ames Research Center. As will be noted in the text to follow, the derived constants differ only slightly.) The heat balance can be represented by the following: heat in is equal to heat stored plus heat discarded. Or, power applied plus heat from powered models equals heat stored in the air plus heat stored in the structure plus heat transferred through walls plus heat discarded through air exchange. That is,

$$P + H_e = (C_p W_a + C_s W_s)\frac{dT}{dt} + \left(\frac{S}{\delta}k + C_p \dot{W}_{ex}\right)(T - T_o) \tag{1}$$

The left side of equation (1) represents the heat input into the system per unit time and the right side expresses how that heat input is absorbed or discarded. Since the walls and supporting structure are made of a variety of materials of different thicknesses, it is difficult to arrive at an average or equivalent value for the parameters C_s, W_s, S, δ, and k. The mass or volume of air contained by the tunnel is, however, of uniform consistency and so is easier to estimate. Based on the dimensions of the facility, the air mass W_a is estimated to be about 900 tons.

Before proceeding with a solution to this differential equation, two limiting situations are considered. At the beginning of a run, the time is t_o and the temperatures of the air in the circuit and of the structure are about the same as the outside ambient temperature, T_o (solar heating, etc., are ignored). The initial rate of temperature rise is then given by equation (1) as (since $T = T_o$)

$$\left.\frac{dT}{dt}\right|_{t=0} = T'_o = \frac{P + H_e}{W_a C_p + W_s C_s} \tag{2}$$

where $(P + H_e)$ represents the heat input per unit time, $W_a C_p$ represents the heat capacity per degree of the air inside the facility, and $W_s C_s$ represents the heat capacity per degree of the structure. Similarly, as the time becomes long, the temperatures of the air in the tunnel and of the structure approach an equilibrium or maximum value asymptotically where $T = T_{max}$ so that the increment above ambient is given by (i.e., for $dT/dt = 0$)

$$(T_{max} - T_o) = \Delta T_m = \frac{P + H_e}{Sk/\delta + C_p \dot{W}_{ex}} \tag{3}$$

Equations (2) and (3) provide conditions at two points on the temperature-time heating curve at which the unknowns are more readily identified and permit the solution to the differential equation to be written as

$$(t - t_o) = \frac{-\Delta T_m}{(dT/dt)|_o} \ln \left[1 - \frac{(T - T_o)}{\Delta T_m}\right] \tag{4}$$

It is assumed, of course, that the energy input from the fan drive and the air-exchange rate are held constant and that the start-up process and arrival at steady-state conditions is done quickly enough so as not to influence the long-term transient. When this is not the case, steady-state power is applied at an initial time t_1 and at a temperature T_1 that is not equal to ambient; as a result, the solution becomes

$$(t - t_i) = - \frac{\Delta T_m}{(dT/dt)|_o} \ln \left[\frac{\Delta T_m - (T - T_o)}{\Delta T_m - (T_1 - T_o)}\right] \tag{5}$$

The initial time t_i is then the beginning time at which the power, heat input, and air exchange reach constant or steady-state values, and T_1 is the temperature of the air and structure at that time.

The foregoing solutions assume that the air and structure are at the same temperature and that the air density is not appreciably changed over the temperature range being considered. It is also assumed that the incoming cool air and the warm air in the circuit are well mixed before the air leaves the exhaust openings. As mentioned previously, exploration of this assumption with the 1/50-scale model of the facility indicated that the residual swirl and turbulence downstream of the six drive fans do an adequate job of mixing. Regions of temperature difference do occur, but they are usually small compared with the increment between the internal and external (or ambient) temperatures. It is also assumed that the temperature of the structure is in equilibrium with that of the tunnel air. This assumption was not checked with the model or at full scale. Obviously, some lag will occur. A portion of the lag will probably be incorporated into the empirical constants for the thermal capacity and conductivity of the structure to be derived in the next section by use of data runs made with the full-scale tunnel.

In the present analysis, it is also assumed that the weight of cooling air being exchanged per second, $\dot{W}_{ex}$, includes the flow of cooling air drawn in through the drive fan motors and exhausted into the wind-tunnel circuit. The volume flow is 40,000 ft^3/min per fan motor, 240,000 ft^3/min total, or 4,000 ft^3/sec. This source of cooling air is constant over the range of power applied to the fan drives and is small compared with the volume of air passing through the air-exchange system at high power (e.g., about 1.4×10^5 ft^3/sec at 10% air exchange). The parameter $\dot{W}_{ex}$ will be used here in the form

$$\dot{W}_{ex} = \dot{m} A_{ts} V_{ts} \rho g \tag{6}$$

where $\dot{m}$ is the ratio of all of the air being exchanged to that flowing through the test section.

Evaluation of Empirical Constants for Temperature-Time Equation

A least-squares method is now used to obtain a best fit to the data from several temperature-time runs made with the full-scale 40 × 80 tunnel (fig. 6). It is to be noted in the data that the start-up transient caused the temperature to begin at values above T_o so that an experimental value for t_o is not available. Also, the first several data points do not line up with the rest of the curve and will be discarded. Therefore, the unknowns to be found by curve fitting are t_o, ΔT_m, and T'_o. For the purpose of the least-squares fit, equation (4) is rewritten as

$$\Delta T_m \ln\left[1 - \frac{T - T_o}{T_m}\right] = t_o T'_o - t T'_o \tag{7}$$

to put it into a form suggested in chapter XI of reference 11 as $y = a + bx$, where $a = t_o T'_o$ and $b = -T'_o$. The logarithmic form for the temperature function y changes the curves in figure 6 into straight lines if the correct values for t_o, T'_o, and T_m are chosen. Since this least-squares approach has the capacity for only two unknowns, a third criterion is obtained in the form of the correlation coefficient R, defined as (e.g., ref. 11)

$$R = b\{[N\Sigma x^2 - (\Sigma x)^2]/[N\Sigma y^2 - (\Sigma y)^2]\}^{1/2} \tag{8}$$

where N is the number of points in the data set.

The technique used to calculate the best values for the three unknowns consisted of an iterative process. A value for ΔT_m was first assumed on the basis of likely asymptotes for the temperatures as $t \to \infty$ for the curves in figure 6. With that value for ΔT_m, the least-squares method was used to find the best values for t_o and T'_o. Both larger and smaller values of ΔT_m were then chosen iteratively to bring the parameter R as close to 1.0 as possible. The corresponding values for t_o, ΔT_m, and T'_o were then taken as the best fit to the data.

Since the input power and the air-exchange rate were known for the data runs, the structural parameters were evaluated. Values obtained by the foregoing process are compared in table 2 with those found by Mort (unpublished analysis, 1974). The two sets of constants are noted to be in fair agreement with one another except for W_sC_s which does not affect the results strongly. The constants to be chosen for the calculations to follow are those obtained by the least-squares/correlation-coefficient technique described in the foregoing paragraphs.

Application to Heating of Tunnel

Although recent changes made in the 40 × 80 tunnel are extensive in the fan drive area, they probably do not alter appreciably the structural composition as it affects the overall heat capacity and heat transfer through the walls. It is assumed, therefore, that the empirical constants derived in the previous section from data taken with the unmodified tunnel also apply to the redesigned facility. The heating equations (1)-(6) are now used to explore how the air temperature in the tunnel is affected by the power applied and by the air-exchange rate. These computations provide a basis for choosing the air-exchange rates needed to carry out various tests without overheating the tunnel. Once the minimum rates have been established, the data can be used in the design of the exchange system.

It is first assumed that the effect of the starting transient on the heating curve is negligible in comparison with the temperature-time history and steady-state temperature asymptote, ΔT_m. Figure 7 illustrates the time-history of the temperature of the tunnel operating at full power (100 MW). Any model in the test section is assumed to be unpowered. Two sets of curves are included to illustrate how the different values for the structural parameters, W_sC_s and Sk/δ, affect the temperature-time history. Although the two sets of curves are not on top of one another, both predict about the same levels of ΔT_m. The maximum, or equilibrium, temperatures are not changed much by the value chosen for the constant Sk/δ, because air exchange dominates the cooling process.

As a supplement to figure 7, the influence of air-exchange rate $\dot{m}$ on the time available for given tests, is shown in table 3 for the tunnel operating at full power with an unpowered model in the test section, and with a model having one or two jet engines operating at full power. The engines are assumed to be J97s which have a heat output of about 10 MW each when operating at full power. Heat added to the airstream by sources in the model is noted to increase significantly the air-exchange rates required to bring acceptable operating times above 30 min.

The ability to run at full drive power on a continuous basis is much more productive than when the test has to be terminated to cool the tunnel, and then restarted. The air-exchange rates estimated by equation (3) to be those required to maintain a given temperature difference between tunnel and ambient temperatures at various power levels (drive power plus heat input from a model engine) are presented in figure 8. These values are essentially independent of the start-up process used to get the test under way and represent the effect of power and ambient air temperature on the required air exchange for steady-state operation. The advantage of

operating on cool days when the temperature difference ΔT_m is larger is apparent in the graph. Conversely, operation of the tunnel on warm days (ambient temperature $\geq$ 90°F) requires significantly larger air-exchange rates.

Application to Cooling of Tunnel

If the heat input from the drive fans and from a powered model is too large for the air-exchange system, the tunnel may reach its temperature limit of 130°F before the test is completed. It will then be necessary to cool the tunnel as quickly as possible so that the test can be resumed. The time required to reduce the tunnel air temperature from near the maximum allowable of 130°F to a lower temperature may be estimated by use of equation (5), if the drive fan power is reduced to a certain value and then held constant. If, for example, the power is reduced to one eighth of the maximum and if the approximation

$$\frac{P}{P_{max}} = \left(\frac{V}{V_{max}}\right)^3 \tag{9}$$

is made, the test-section speed is about one half of 300 knots, 150 knots. Typical values estimated for the time required to reduce the temperature of the air in the tunnel and of the structure to a lower temperature is presented in table 4. It is noted that the tunnel cools quickly at first and then more slowly as it approaches the equilibrium temperature for that power setting.

Since the cooling process is downtime for the tunnel test, it is important to reduce the time required to a minimum. One way to achieve this is to run the tunnel at the velocity or power which maximizes the cooling rate for the temperatures of the tunnel and of the ambient air that exist at that instant. Since the heat input is proportional to applied power, or velocity to the third power, and since the rate of flow of cooling air is proportional to tunnel velocity to the first power, the optimum power is a balance between the two. Such an optimum is found by differentiating equation (1) with respect to power, and setting the parameter $d(dT/dt)/dP$ equal to zero. When equations (6) and (9) are inserted into equation (1), it becomes

$$P = (W_a C_p + W_s C_s)\frac{dT}{dt} + \left[\frac{Sk}{\delta} + C_p \dot{m} V_{ts} A_{ts} \rho g\right](T - T_o) \tag{10}$$

After differentiation with respect to P and setting $d(dT/dt)/dP = 0$, the optimum power setting P_{opt}, to be used to cool the tunnel at a given instant, is given by

$$\frac{P_{opt}}{P_{max}} = \left[\frac{C_p \dot{m} V_{max} A_{ts} \rho g (T - T_o)}{3P_{max}}\right]^{3/2} \tag{11}$$

The optimum power is noted to vary only with the air-exchange rate and with the temperature of the tunnel above ambient. Once the inlet and exhaust openings are set, the air-exchange rate $\dot{m}$ is a constant independent of power (or test section velocity); however, the temperature difference $(T - T_o)$ changes continuously as the tunnel cools. Therefore, the most rapid cooling process is to vary the power continuously as the tunnel temperature comes down so that the power is always at the optimum value for cooling. When the optimum power relationship is inserted into equation (1) and the integration is carried out, the minimum time to cool the tunnel to a desired temperature is given by

$$(t - t_i) = 2\left(\frac{W_a C_p + W_s C_s}{Sk/\delta}\right) \ln \left| \frac{Sk/\left(\delta\sqrt{\Delta T}\right) + \left(2/\sqrt{P_{max}}\right)[C_p \dot{m} V_{max} A_{ts} \rho g/3]^{3/2}}{Sk/\left(\delta\sqrt{\Delta T_i}\right) + \left(2/\sqrt{P_{max}}\right)[C_p \dot{m} V_{max} A_{ts} \rho g/3]^{3/2}} \right| \quad (12)$$

where $\Delta T = T - T_o$, and $\Delta T_i = T_i - T_o$.

The operating procedure needed to vary the power continuously as the tunnel cools will no doubt be cumbersome. It is desirable then to know how much time is saved by the continuously varying process over that of cooling at a single setting. A comparison is made in table 4 of the optimum or continuously varying case (eq. (12)), with several fixed power cases (eq. (5)). It is to be noted that for the cases shown, not much difference occurs until the tunnel temperature is reduced to near ambient or to near the equilibrium temperature for the power setting being used to cool the tunnel. An alternative method, for example, would then be to use two power settings for a cooling cycle instead of either one setting or a continuously varying one. The first of the two settings could be at $P_c = P_{max}/8$ and the second at $P_c = P_{max}/64$; $(V_c = V_{max}/4)$. The equilibrium temperatures for the two values of P_c are $\Delta T_m = 12.0°F$ and $\Delta T_m = 2.2°F$, respectively, when $\dot{m} = 0.05$. A two-step process such as this one would make it possible to cool the tunnel down to temperatures near ambient almost as rapidly as with the continuously varying process.

ANALYSIS OF FULL-SCALE DATA FOR AIR-EXCHANGE RATE

As mentioned previously, tests were conducted in 1982 with the full-scale facility to prepare it for implementation. Although a large amount of data was taken during these tests, a direct measurement of the air-exchange rates was not obtained for the various test configurations. The data available that have a bearing on the performance of the old air exchanger are the test-section velocity and the pressures in the north and south legs of the tunnel relative to the atmosphere. Since an understanding of the old exchanger would be helpful in the design of the new one, the 1/50-scale model was used to calibrate and analyze the full-scale system which was in existence at the time of the 1982 tests. This required that the model tunnel be configured to duplicate the full-scale one as closely as possible (figs. 1, 2, 4). The three exhaust ports in the model were covered with a screen (81% porosity) and with brass bars estimated to have about the same loss

coefficient as the bird and debris screen and superstructure of the full-scale tunnel (fig. 2(b)). It was assumed then that the flow rate through each orifice of the model is related to the pressure drop across it in the same way as in the full-scale facility. In the model, the pressures were measured with water manometer boards and the flow rate with a commercially available flow-rate meter designed for heating and air conditioning systems. The calibration on the flow-rate meter was checked with pitot tube surveys and found to be accurate to within about 5%. For the calibration of the exhaust ports, the flow into the tunnel was controlled by opening a door-type inlet located in the north leg of the model tunnel. The inlet and exhaust openings in the model had to be calibrated separately, because the pressure drop from the south to the north legs is different in the model and full-scale tunnels; that is, $(p_s - p_n)/q_{ts} = 0.285$ for the model and $(p_s - p_n)/q_{ts} = 0.24$ for the full-scale tunnel.

The flow rate through the exhaust ports which simulate the 1982 tests is presented in figure 9 as a function of the difference in total pressure across the south wall for a range of tunnel speeds and inlet door openings. It was found that even though the velocity along the south leg is relatively small, it appears to be large enough to influence the flow rate. Therefore, acceptable correlation of the data required the use of total rather than static pressure in the south leg. Use of the total pressure causes the data to fall on a nearly straight line much like that for classical orifices. Unlike classical orifice theory, however, the exponent of the pressure curve for the screened orifice is about 0.62 rather than 0.5, so that the flow-rate relationship for the exhaust ports is given by

$$\dot{m} = 0.18[(H_s - H_{atm})/q_{ts}]^{0.62} \tag{13}$$

where H_{atm} is atmospheric pressure.

A similar calibration was then made of the old-style inlet orifices in the north leg of the model tunnel. The door inlets were first simulated with openings of the same shape as that of the full-scale ones. Since it was not possible to duplicate the complex details of the full-scale louvers and screens at small scale, the pressure drop across the opening was simulated with multiple layers of screen of 71% porosity. The flow rate through an inlet orifice was then found to be approximated by

$$\dot{m} = 0.15[(H_{atm} - p_n)/q_{ts}]^{1.0} \tag{14}$$

It is to be noted that the exponent is now 1.0 rather than 0.5 and that the data correlate best with the static rather than with the total pressure in the north leg.

The foregoing calibrations made it possible to infer the air-exchange flow rates that occurred during the 1982 full-scale tests. The data presented in table 5 indicate that values of $\dot{m}$ as high as 0.05 (5% air exchange) were probably achieved. As mentioned previously, the static-pressure differential between the north and south legs of the circuit is nearly constant over configuration changes and tunnel speeds. At full-scale, the pressure differential is 0.24. The

corresponding differential for the 1/50-scale model is about 0.285. The difference in these two measured pressure differentials is attributed to the small scale and low Reynolds number of the model tunnel, which lead to higher losses in the east leg and through vane sets Nos. 8 and 1. These scale and Reynolds-number effects cause the model to have a larger pressure difference between the north and south legs than observed for the full-scale facility.

EFFECT OF AIR-EXCHANGE INLET CONFIGURATION ON TEMPERATURE AND DYNAMIC PRESSURE PROFILES

On the basis of the discussion in a previous section (General Considerations), the two contoured inlets in the north leg of the circuit and the inlets used during the 1982 Integrated Systems Test (IST) were tested with the 1/50-scale model of the 40 × 80 tunnel. The exhaust system used for these tests consisted of five openings in the southwest corner of the circuit which simulated five doors removed from the westernmost column of vane set No. 7 in the full-scale device; figure 2(b) shows the three doors removed for the 1982 IST. The data surveys chosen to be presented provide information for choosing the inlet configuration to be used in subsequent tests and in the full-scale facility.

The temperature profiles in the tunnel circuit were found to be insensitive to the manner in which the air was introduced into the circuit. That is, the six drive fans apparently mix the airstream to such an extent that the cool air from the inlet is no longer a well-defined stream tube. The mixing is not complete, however, because a slightly different temperature profile occurs across the test section when the air is all taken in through the north-wall inlet as compared with when it is all taken in through the courtyard wall inlet (fig. 10). Although the two curves for 10% air exchange ($\dot{m} = 0.1$) differ, a systematic temperature gradient did not occur, and the maximum excursion in the temperature across the test section is less than 2°F, which is within the allowable temperature difference.

Measurements were then made to find out how the total head profiles were affected by the different inlet schemes for the cooling air. These measurements consisted of total head profiles across the tunnel circuit at various stations of interest. Since static pressure in the tunnel depends strongly on the air-exchange rate, the plots are shown as dynamic pressure rather than total head to provide a more direct comparison between configurations. That is, the dynamic pressure q was taken as the total head H minus the local static pressure p, as measured on the walls at that station. The effect of air-exchange rate and exhaust configuration on static pressures in the north and south legs of the facility are treated in the next section.

The dynamic pressure head just downstream of the contoured inlets is presented in figure 11 for three different inflow geometries. The energy of the incoming jet is clearly evident by the approximately rectangular segment in the profile for the two upper curves. Injection of higher-energy air along the walls provides a boost

to the low-energy air in the boundary-layer flow at that station. The diffusion of these jets of air as the streams proceed downstream through vane set No. 2 and around the northwest corner of the circuit toward the fans is reflected in the profiles presented in figure 12. The lowest curve, which is for $\dot{m} = 0$, indicates the increase in the amount of sluggish flow entering the fans along the inside of the circuit. Introduction of all of the cooling air through the courtyard contoured opening produces significant benefit to the profile by making it more uniform because of the boost it gives to the low-energy flow near the courtyard wall. Conversely, injection of the cooling air through the opening in the north wall does not make the velocity profile entering the fans much more uniform because the flow along the outside wall is already fairly robust. The top curve was made by allowing about equal amounts (i.e., $\dot{m} = 0.05$ per inlet) of air through the north wall and courtyard inlets. As expected, the flow along the outer or north and west walls is not improved significantly, and the improvement realized along the courtyard wall is notable but not equal to that produced when all of the air is introduced through the courtyard inlet (fig. 12).

The results in figures 11 and 12 confirmed the expectation that the courtyard inlet is the best configuration because it is the one that provides the maximum benefit to the velocity profile of the flow entering the drive fans. That is, the incoming air jet boosts the velocity along the courtyard wall to such an extent that the profile becomes more nearly uniform than by any other injection scheme tested. The beneficial aspects are further illustrated in figure 13 where the dynamic pressure profiles for two inlet configurations are compared with the no-air-exchange case. As mentioned previously, the inlets used during the 1982 IST induce further degradation in the profile along the courtyard wall rather than building up the energy of the flow field there. It is concluded, therefore, that the 1982 IST air-exchange system should be removed and replaced with a contoured courtyard inlet.

Finally, the effect of air exchange on the dynamic pressure distribution across the test section is negligible, as shown in figure 14. In a series of tests which followed the present measurements, it was discovered that the asymmetry in the profile shown in figure 14 is brought about by underturning of the air through vane set No. 6 (cf. ref. 9) and is not due in any way to the exchange of cooling air. Measurements were also made in other parts of the circuit to be sure that the flow was not degraded by the use of only the contoured courtyard inlet. No adverse effects were found. None of these additional plots is presented here because they were not obtained with the model tunnel configured to duplicate precisely the final facility.

EFFECT OF AIR-EXCHANGE RATE AND EXHAUST CONFIGURATION ON WALL PRESSURES

The previous section dealt with the effect of the air-exchange inlet on the distribution of temperature and total head at various stations in the circuit. In this section, the effect of the exhaust opening and air-exchange rate on the static pressures in the north and south legs of the circuit are analyzed using experimental

data from the model tunnel. The wall pressures are of concern because the walls are designed to withstand only a given differential pressure. The exhaust configurations were openings in the westernmost column of vane set No. 7 which consisted of the following door arrangements:

1. Three door panels removed, that is, the configuration used during 1982 IST; area $\approx 18 \times 11 \times 3$ ft $= 594$ ft^2.

2. Five door panels removed; area ≈ 990 ft^2.

3. Six doors in upper half of column opened at design angles to deflect exhaust jet upward at about 40°; effective area $\approx 1188 \sin(90° - \theta) = 910$ ft^2. The parameter θ is the angle at which the exhaust jet is deflected upward by the doors.

4. Entire column of 11 1/2 doors opened at design angles to deflect exhaust upward at about 40°; effective area $\approx 2277 \sin(90° - \theta) = 1{,}744$ ft^2.

One door panel is approximately 18 × 11 ft or 198 ft^2.

As noted in the list, the size of the exhaust opening is regulated by changing the number of doors open. Another option is to choose other panels in vane set No. 7 for removal or opening. This possibility was not explored because it did not seem likely that such an exhaust opening would enhance appreciably the uniformity of the circuit airstream. Also, a contoured surface, like the one used for the inlet, to guide the exhaust air more smoothly from the tunnel was not tried; little benefit was expected because of the low dynamic pressure of the airstream in the south leg of the tunnel (i.e., $\lesssim 4.5$ lb/ft^2) and because of installation difficulties.

To simplify the operation of the air-exchange system and to reduce the likelihood of inadvertent overpressurization of the facility, a decision was made to build the exhaust openings in a fixed position. Only the inlet opening is variable then, so that changes in air-exchange rate are accomplished by changing the amount of door opening of the inlet. As recommended in the previous section, all data from now on were taken by using only the courtyard contoured inlet door, which directs the incoming cooling-air jet downstream in a smooth efficient manner. Usually, a screen to prevent ingestion of debris was not used over the inlet because it did not significantly alter the flow rate and it did interfere with the measurement technique. A screen and simulated superstructure were located over the exhaust orifices to simulate the interference to be encountered full scale.

The first measurements to be discussed are the flow rates obtainable with the four exhaust openings listed above (fig. 15). The curves were obtained by setting up a given exhaust configuration and then changing the flow rate by opening or closing the inlet door. It is to be noted that as the inlet door is opened to allow larger air-exchange rates, the pressure inside the tunnel increases so that an increased flow rate is induced through the exhaust ports. As the pressure builds, the larger back pressure reduces the inflow rate. Equilibrium is reached when inflow equals outflow. As expected then, a nearly linear relationship between door

opening and flow rate exists only at the lower flow rates. At the larger flow rates, the flow rate increases only a small amount with door opening because of the buildup of back pressure. It is to be noted in figure 15 that both the air-exchange rate and door opening are in dimensionless units. Since the north leg of the wind tunnel is 108.6 ft across, a 1% opening corresponds roughly to a 1.09-ft increment in door opening.

Measurements of the static pressure in the north and south legs of the tunnel were then made for a range of inlet door openings with each of the four exhaust configurations. As mentioned in prior sections and as indicated in figure 16, the model and full-scale pressures differ in the north leg. The measurements made with the 1/50-scale model and plotted in figure 16 and in the next few figures to follow have been adjusted to the maximum velocity anticipated for the full-scale tunnel, that is, V_{max} = 300 knots and $q_{ts\ max} \approx 274$ lb/ft^2. Such a scale is used to facilitate discussion of the maximum loading to be expected on the walls of the tunnel for the various inlet and exhaust designs.

The wall-pressure data for all four exhaust sizes and for the 1982 IST system are presented in figure 17. Not accounted for in the data from the model (i.e., open symbols) is that the cooling air which flows directly through the drive motors does not enter through the inlet but does exit through the exhaust openings. The total flow rate through the six motors is a constant at 4,000 ft^3/sec. In addition, both the 1/50-scale model and the full-scale facility have air leaks. Although the two sources of airflow are small, they affect the so-called zero flow rate. Even so, since the exhaust openings are large, the pressure differential resulting from these factors is small.

The difference in the model and full-scale pressures in the north leg for three doors removed is believed to be caused by the differences in scale and Reynolds number. Interpretation of the model data for the internal pressures that load the walls requires that the model data be adjusted to full scale. It was reasoned that the drag difference between the two wind tunnels could be scaled by the ratio of the two values at zero flow rate. Namely, if the pressures measured with the model are first scaled to maximum velocity, as shown in figure 17, and then multiplied by 70/80, the 1982 IST data and the data from the model for three doors open are in agreement (fig. 18). The curves for the other exhaust openings also take on a more consistent character.

The information in figure 18 can now be used to explore the relationship between the size of the exhaust opening and air-exchange rate when the pressures in the north and south legs of the facility are designed to specified limits. Consider first the limits used in 1982 which allowed pressures as low as -55 lb/ft^2 in the north leg and as high as +18 lb/ft^2 in the south leg. As indicated in figure 19(a), each pressure limit requires that the air-exchange rate lie between the two curves shown there. That is, for a small exhaust opening (say three doors removed), the air-exchange rate is restricted to values between about 2.5% and 3.75%. If five panels are opened for the exhaust, the air-exchange rate can safely be varied between about 4.2% and 6.4%. Larger exhaust openings permit larger values of $\dot{m}$, but the excursion of $\dot{m}$ between limits does not increase a great deal for the case

shown in figure 19(a). Figures 19(b) and 19(c) illustrate how the air-exchange rates change as the tolerable pressure is increased or decreased. Since the design limits have now been set at -64 lb/ft^2 and +18 lb/ft^2, the curves in figure 20 apply to the full-scale tunnel. Modifications of the curves to account for the power limit of 100 MW will be discussed in the next section.

Consideration in the final design must be given to the possibility that cladding material will be lost at some time from either the north or south legs of the tunnel. In such an event, the newly opened area will in effect increase the size of the inlet or exhaust of the air-exchange system. In order to estimate the changes in wall pressures that would occur in such a case, the data in figure 18 were used to obtain the curves shown in figure 21 for two air-exchange rates (5% and 6%) likely to be used at maximum tunnel speed. The advantages in safety for the south end when designed to +18 lb/ft^2 with a large exhaust opening (i.e., entire west column open) are immense in the event that cladding is lost on the north leg. A design pressure in the north leg of -70 lb/ft^2 would ensure that a loss of cladding on the south leg would not also jeopardize the north end. Since the design pressure is -64 lb/ft^2, the air-exchange rates allowable will have to be restricted to values larger than a given amount.

The various exhaust openings do disrupt the flow in the southwest corner of the facility where vane set No. 6 intersects the corner, but this effect was not studied in detail. The flow disturbances appear to persist along the south wall of the south leg for some distance and may even cause increased turbulence along the eastern wall of the test section. Nevertheless,these disadvantages did not appear great enough to warrant an extended study of other exhaust configurations.

ESTIMATE OF POWER REQUIRED TO SUPPORT AIR EXCHANGE

Expressions are derived in this section for the losses that occur when air is being exchanged. Comparison with available experimental results is made where possible. The approximate formulas derived here are then used to predict power changes required by air exchange and to investigate ways to minimize the power required. The various power-loss components are determined as a fraction of the power required to drive the wind tunnel when there is no air exchange. Under those circumstances, the power required is

$$P_o = V_{ts} q_{ts} A_{ts} \sum K_D \tag{15}$$

where the drag of the entire circuit, without air exchange, as (cf. ref. 8)

$$C_{Do} = \sum K_D = 0.176 \tag{16}$$

The power loss associated with the air-exchange system for the 40 × 80 tunnel is separated into four categories:

1. Inlet losses: obstructions to the incoming flow such as screens, struts, superstructure, and louvers; and turning losses

2. Increase in circuit drag brought about by increase in volume of flow from inlet to exhaust

3. Pressure energy discarded with exhaust air into the atmosphere

4. Changes in fan or circuit performance caused by air exchange

These four items will be considered in the following subsections as increments in the power needed to support air exchange.

Inlet Losses

The first of the inlet losses to be considered is the one incurred at the coarse screen of large porosity (usually of 70% to 80%) over the inlet opening to keep trash, birds, and various debris from entering the circuit. Since these screens have a low (about 0.2) loss coefficient (ref. 12, p. 31 indicates a range of loss coefficients of $\Delta H/q_{local}$ = 0.1 to 0.3) and the velocity is small at the screen surface, $q_{local}/q_{ts} \approx 0.1$, the total head loss of the incoming air, which is attributable to what is generally referred to as the "bird screen," is estimated as

$$\frac{\Delta H}{q_{ts}} \approx 0.2 \times 0.1 = 0.02 \tag{17}$$

Similarly, the loss caused by the superstructure, which supports the wall of the tunnel and cannot generally be removed or moved elsewhere, is for the present purposes estimated to be about the same as that of a second bird screen, that is,

$$\left.\frac{\Delta H}{q_{ts}}\right|_{\text{bird screen}} + \left.\frac{\Delta H}{q_{ts}}\right|_{\text{superstructure}} \approx 0.04 \tag{18}$$

When these two sources of loss are referred to the power used to drive the tunnel, the power fraction devoted to the inlet interference is given by

$$\frac{\Delta P_{bs}}{P_o} = \frac{\text{Power absorbed by inlet interference}}{\text{Power required to drive tunnel}}$$

$$= \frac{0.04\dot{m} \cdot A_{ts} \cdot q_{ts} \cdot V_{ts}}{\sum K_D \cdot A_{ts} \cdot q_{ts} \cdot V_{ts}} = \frac{0.04\dot{m}}{0.176} \approx 0.2\dot{m} \tag{19}$$

The second loss that is incurred near the inlet arises from the mixing and dissipation which occur as the air is turned from the incoming direction, which is

perpendicular to the circuit centerline, to a direction parallel to the circuit centerline. Observations with smoke in both the full-scale and model tunnels indicated that the louvered-type inlet used during the 1982 IST injected the air into the circuit as a transverse jet with high turbulence so that most, if not all, of the kinetic energy of the air was lost on entry (fig. 3). In such a case, the upper limit of the loss is assumed to be equal to the entire kinetic energy of the incoming air, or

$$q_{air\ jet} \approx p_{atm} - p_{no.\ end} \tag{20}$$

The extra power, ΔP_{louv}, required to compensate for such a loss is then given by

$$\frac{\Delta P_{louv}}{P_o} = \frac{(p_{atm} - p_{no.\ end})\dot{m}A_{ts}V_{ts}}{q_{ts}A_{ts}V_{ts}\sum K_D}$$

$$= \frac{p_{atm} - p_{no.\ end}}{q_{ts}} \frac{\dot{m}}{\sum K_D} \approx \frac{\Delta p\ \dot{m}}{q_{ts}C_{D_o}} \tag{21}$$

If, however, a contoured panel or door and wall shaping is used to turn the air, as is planned for the remodeled facility, the entire dynamic pressure can be recovered (fig. 11) so that the turning loss for the contoured inlet becomes negligible, or

$$\frac{\Delta P_{cont.\ inlet}}{P_o} \approx 0 \tag{22}$$

Power Loss Increment Caused by Extra Circuit Drag

After the cooling air has entered the circuit, it moves downstream through vane set No. 2, along the west leg of the circuit, through the drive fans to the exhaust ports in the southwest corner of the facility. As a result, the volume of air flowing along that part of the circuit is proportionately larger by $\dot{m}$ than in other segments of the circuit. The penalty in circuit drag and power incurred because of the higher flow rate can be expressed as an incremental increase over the power when there is no air exchange. That is, from equation (15),

$$P_o = C_{Do}q_{ts}A_{ts}V_{ts}$$

when there is no air exchange, and, when $\dot{m}$ is not zero,

$$P_o + \Delta P_{circ} = (C_{Do} - C_{Dw})q_{ts}A_{ts}V_{ts} + C_{Dw}[q_{ts}(1 + \dot{m})^2][V_{ts}(1 + \dot{m})]A_{ts} \tag{23}$$

where C_{Dw} is the drag coefficient of the western part of the circuit through which the increase in cooling air flow occurs. It is assumed that the fan performance is

not affected by the added mass flow. The change in power required to support the added drag and velocity in the circuit may then be written as

$$\frac{\Delta P_{circ}}{P_o} = \frac{C_{Dw}}{C_{Do}} [3\dot{m} + 3\dot{m}^2 + \dot{m}^3]$$

Since $\dot{m} \lesssim 0.1$, and since $C_{Dw}/C_{Do} \approx 0.5$, the power increment may be approximated by

$$\frac{\Delta P_{circ}}{P_o} \approx \frac{3\dot{m}}{2} \tag{24}$$

Pressure Energy Discarded with Exhaust

The air leaving the circuit through the exhaust openings does so with a velocity and a pressure sufficient to overcome the drag of the orifice, the back pressure of the atmosphere, and the dynamic pressure of the issuing jet. An estimate of these losses is obtained by assuming that the portion of the total head of the jet H_j that is in excess of atmospheric pressure constitutes the loss. That is,

$$\frac{\Delta P_{exh}}{P_o} = \frac{(H_j - p_{atm})/q_{ts}}{C_{Do}} \cdot \dot{m} \tag{25}$$

An expression for H_j could probably be derived from the orifice coefficient, but it is more convenient and more accurate to measure the quantity $\Delta H_j/q_{ts} = (H_j - p_{atm})/q_{ts}$ directly with the 1/50-scale model of the wind tunnel. The power loss estimated for the expelled air by this method is presented in figure 22 for the several different exhaust openings studied here. As expected, the smaller openings quickly induce high losses as $\dot{m}$ increases. Also shown in the figure is a straight line representing the $\Delta P_{circ}/P_o = 3/2\dot{m}$ power increment required to compensate for the extra drag along the western half of the circuit that is caused by the air exchange.

Comparison with Experiment

A comparison with data is now made to evaluate the accuracy of the foregoing equations for estimating the power lost because of various factors involved in the air exchange. All of the equations ignore any temperature changes or differences that may exist because of the approximate nature of the estimates. The data obtained during the 1982 IST are first compared in figure 23 with the three increments for power loss. The full-scale data are quite widely scattered so that a definitive decision on the accuracy of the equations is not possible. However, the sum of the three components represented by the uppermost curve is in good agreement with the larger values of power loss. Overall, the trends and magnitude are close

enough to suggest that the theoretical estimates are about correct. Needless to say, it is disconcerting to realize that an air-exchange rate of 5% probably absorbed about 15% of the power required to drive the tunnel during the 1982 IST. As noted earlier, however, the power loss can be reduced by use of an improved inlet and larger exhaust openings.

An indirect measurement of the power absorbed by air exchange was then made with the 1/50-scale model of the tunnel by observing the change in dynamic pressure in the test section as air exchange was turned on and off (fig. 24). Comparison of these results with the theoretical estimates is questionable because the six drive fans were sensitive to air-exchange rate. That is, since the pitch of the fans is fixed and since they are working close to stall, their performance is sensitive to the uniformity of the flow coming into the station where the fan faces are located. As mentioned previously, the incoming air provides a boost to the boundary layer on the courtyard side of the circuit so that the velocity profile entering the fans is more uniform when air exchange is in progress. The improved fan performance compensates somewhat for the increased power lost in the air exchange. The data points and the theoretical curves shown in figure 24 appear to have some sort of compensating process such as the one just described, which causes the discrepancy between the results. It is concluded that the 1/50-scale model is not well suited to a test for the estimated power relationships and that the increments in power loss derived here probably provide acceptable engineering accuracy.

Since the power required to support air exchange is sizable, consideration was given to ways by which losses could be reduced. The inflow losses at the inlet have already been essentially eliminated by the contoured wall and inlet door changes. Removal of screens and superstructure which obstruct the inflow and outflow are unacceptable reduction schemes. The losses along the western part of the circuit where the volume flow of air is increased by $(1 + \dot{m})$ could be reduced by shortening the length of the circuit along which the cooling air must flow between inlet and exhaust; that is, by locating the exhaust ports nearer to the inlet. Such an alternative causes many structural problems, however, and may make certain operational procedures difficult. Since none of the concepts appeared more promising than the ones considered here, no further testing was carried out.

OPERATIONAL CONSIDERATIONS BROUGHT ABOUT BY AIR EXCHANGE

Several ways in which air exchange affects the operational procedures of the facility are discussed in this section. Consideration is given to these items because they affect the test-section performance available for investigations and the integrity of the structure.

The first item to be analyzed is the reduction in the available velocity and dynamic pressure to be expected in the test section when the courtyard contoured door and wall are used as the inlet with various exhaust configurations. It is

assumed that the power, velocity and dynamic pressure in the test section are related by

$$\frac{P}{P_{max}} = \left(\frac{V}{V_{max}}\right)^3 = \left(\frac{q}{q_{max}}\right)^{3/2} \tag{26}$$

Based on such an assumption and on the foregoing estimates of the power increments required to support air exchange, the changes in maximum performance were estimated as shown in figure 25. The advantages of the larger exhaust openings are apparent.

The consequences of reduced maximum velocities on wall pressures is considered next. The curves in figures 17 and 18 assumed that the tunnel had the capacity to operate at $q_{ts} = 274$ lb/ft^2 at all values of $\dot{m}$. Since considerable power may be absorbed by exchanging air, the curves in figure 18 were recalculated to include the reduced performance expected at nonzero air-exchange rates. It was therefore assumed that the tunnel is capable of $q_{ts} = 274$ lb/ft^2 only when there is no air exchange. (The maximum test section velocity achieved during the 1982 IST was about 268 knots. Since the losses in the tunnel circuit will have been reduced by the proposed modifications, there is a chance that the revised facility will come close to $V_{ts} = 300$ knots and $q_{ts} = 274$ lb/ft^2.)

The pressures in the north and south legs as a function of air-exchange rate were then modified to reflect the fact that the maximum velocity in the test section is limited by the maximum power available (100 MW) rather than assuming $q_{ts} = 274$ lb/ft^2 for all cases. Such a consideration was investigated to find out if the structure was capable of sustaining the aerodynamic loads while operating at full power rather than at a fixed q_{ts}. When the curves in figure 25 are combined with those in figure 18, the pressures expected in the north and south legs of the facility at various air-exchange rates are calculated as shown in figure 26. The curves are noted to change somewhat, but not to the degree required to significantly reduce the maximum design pressures for the walls. The changes are more apparent in figure 27 where the information in figure 20 is compared with the curves generated with the revised data in figure 26. It is to be noted that the power limit has only a negligible influence until the larger air-exchange rates are used. The boundary imposed by the maximum opening possible with the inlet door is presented in figure 28.

The data presented in the foregoing figures suggests that the best exhaust opening is the largest one studied. The use of air-exchange rates of 5% or more are then permissible at all possible operating speeds if the north leg is designed to -64 lb/ft^2 and the south leg to +18 lb/ft^2. A safety interlock is then only needed to ensure that the air-exchange rate is above about 4.8% when the tunnel is taken to its maximum power of 100 MW.

STEADY-STATE AERODYNAMIC LOADS ON INLET OF AIR EXCHANGER

To obtain estimates of the aerodynamic loads on the structure in the vicinity of the inlet door to the air exchanger, a two-dimensional, potential-flow model of the inlet was developed. The predictions of the potential-flow model were first compared with the experimental results from the 1/50-scale model, and empirical adjustments were then applied. This procedure provided estimates for the aerodynamic loads on the inlet door, on the inlet fairings, and on the external bird and debris screen.

The potential-flow code chosen to model the air-exchanger inlet was POTENT (ref. 13), a code that has been used extensively to model several other aerodynamic components of the NFAC. Figure 29 shows a representation of the two-dimensional flow field of the inlet as modeled by POTENT. Important features to note are the uniform upstream and downstream velocity profiles and the fact that the internal total pressure is equal to atmospheric pressure. Figure 30 presents a schematic of the actual internal flow. Features not simulated in the potential-flow model are the nonuniform upstream and downstream velocity profiles that are caused by the relatively thick boundary layer on the walls of the wind tunnel. Additionally, in the actual tunnel the average total pressure will not necessarily be equal to atmospheric pressure. As a result, the wall jet velocity will not always match the mean channel velocity as will be the case in the potential-flow analysis.

In order to compensate for the inability of the theoretical analysis to account for the foregoing boundary-layer and multi-energy effects, the theoretical results were adjusted on the basis of data obtained with the 1/50-scale model of the facility. In effect, the theoretical results at one condition were assumed to be applicable at another by making the experimental and theoretical zero-hinge-moment positions of the door agree. In the experiment, the zero-hinge-moment position of the inlet door was taken as the location to which it opens if allowed to swing freely on its hinge. This position, referred to as the neutral point, varies with tunnel operating conditions. The measured neutral point appears to correlate best with the difference between the upstream static pressure and atmospheric pressure normalized by the upstream dynamic pressure (fig. 31). Note that the data at a pressure ratio of 1.35 were all taken when the fan drives on the inside of the wind-tunnel circuit were stalled. This stalled condition represents the worst conceivable operating condition for the inlet door (the single point at 22 ft was considered to be extremely unlikely in the full-scale facility). The predicted door moments as a function of door opening are presented in figure 32 along with the adjustments in the door opening required to bring the two-dimensional potential-flow predictions into agreement with the experimental worst-case, neutral-point position. The estimated pressures across the inlet door are shown in figure 33 as a function of the adjusted door opening. These values are based on a design value for an upstream static pressure of 64 lb/ft^2 below atmospheric.

The aerodynamic load on the bird and debris screen and on the inlet fairing do not require any adjustment for the internal flow variations. They were, therefore,

taken directly from the two-dimensional potential-flow predictions for the assumed internal static pressure of 64 lb/ft^2. The pressure distribution on the vertical fairing is shown in figure 34. The pressure distribution on the upper and lower fairings, which are horizontal, are assumed to have the same shape as that of the vertical fairing, even though the flow direction differs. However, the magnitude of the pressure distributions is empirically adjusted in proportion to the peak pressures shown in figure 35. Finally, the dynamic pressure distribution at the location of the bird and debris screen, as predicted by the potential-flow code, is given in figure 36. The loads on the screen depend on the loss coefficient of the screen chosen for the full-scale facility.

CONCLUDING REMARKS

A 1/50-scale model of the 40- by 80-Foot Wind Tunnel at Ames Research Center was used to study various air-exchange configurations. System components were tested throughout a range of parameters, and approximate analytical relationships were derived to explain the observed characteristics. It was found that the efficiency of the air exchanger could be increased by adding a shaped wall to turn the incoming air downstream smoothly, by changing to a contoured door at the inlet to control the flow rate, and by increasing the size of the exhaust opening. The static pressures inside the circuit then remain within the design limits, if the air-exchange rate is about 5% or more at the higher tunnel speeds. Since the model is much smaller than the full-scale facility, it was not possible to completely duplicate the tunnel and it will be necessary to measure flow rate, tunnel pressures, etc. during the IST of the remodeled facility. The aerodynamic loads on the remodeled inlet were also estimated using a potential-flow code in conjunction with the 1/50-scale model of the facility.

REFERENCES

1. Pope, Alan; and Harper, John J.: Low-Speed Wind Tunnel Testing. John Wiley & Sons, Inc., New York, 1966.

2. Eckert, William T.; Mort, Kenneth W.; and Piazza, J. E.: Wind-Sensitivity Studies of a Non-Return Wind Tunnel with a 216- by 432-mm (8.5- by 17.0-in) Test Section. Phase I. NASA TM X-62,171, 1972.

3. Eckert, William T.; Mort, Kenneth W.; and Piazza, J. E.: Wind-Sensitivity Studies of a Non-Return Wind Tunnel with a 216- by 432-mm (8.5- by 17.0-in) Test Section. Phase II. NASA TM X-62,307, 1973.

4. Mort, K. W.; Eckert, W. T.; and Kelly, M. W.: The Steady-state Flow Quality of an Open Return Wind Tunnel Model. Can. Aeronaut. Space J., vol. 18, no. 9, Nov. 1972, pp. 285-289. (See also NASA TM X-62,170, 1972.)

5. Kelly, M. W.; Mort, K. W.; and Hickey, D. H.: Full-Scale Subsonic Wind Tunnel Requirements and Design Studies. NASA TM X-62,184, 1972.

6. Mort, Kenneth W.; Soderman, Paul T.; and Eckert, William T.: Improving Large-Scale Testing Capability by Modifying the 40- by 80-Ft Wind Tunnel. AIAA J. Aircraft, vol. 16, no. 8, Aug. 1979, pp. 571-575.

7. Eckert, William T.; and Mort, Kenneth W.: Wind vs. Wind Tunnel: The Aerodynamics of the Inlet for NASA's New Very Large, Non-Return-Flow Facility. J. Wind Eng. Ind. Aerodyn., vol. 9, no. 3, Mar. 1982, pp. 193-205.

8. Mort, K. W.; Engelbert, D. F.; and Dusterberry, J. C.: Status and Capabilities of the National Full-Scale Facility. AIAA Paper 82-0607, 1982.

9. Corsiglia, Victor R.; Olson, Lawrence E.; and Falarski, Michael D.: Aerodynamic Characteristics of the 40- by 80-/80- by 120-Foot Wind Tunnel at NASA Ames Research Center. AIAA Paper 84-0601, San Diego, Calif., 1984. (See also NASA TM-85946.)

10. Rossow, V. J.; Schmidt, G. I.; Reinath, M. S.; Van Aken, J. M.; Parrish, C. L.; and Schuler, R. F.: Experimental Study of Flow Deflectors Designed to Alleviate Ground Winds Induced by Exhaust of 80- × 120-Foot Wind Tunnel. NASA TM-88195, 1986.

11. Worthing, Archie G.; and Geffner, Joseph: Treatment of Experimental Data. John Wiley & Sons, Inc., New York, 1943.

12. Hoerner, Sighard F.: Aerodynamic Drag. The Otterbein Press, Dayton, Ohio, 1951.

13. Olson, L. E.; James, W. D.; and McGowan, P. R.: Theoretical and Experimental Study of the Drag of Single- and Multielement Airfoils. J. Aircraft, vol. 16, no. 7, July 1979, pp. 462-469.

TABLE 1.- TYPICAL TEST TIMES REQUIRED TO OBTAIN DATA

Powered lift	
$V_\infty \approx$ 50-150 knots (small amount at 300 knots)	
Time scenario	
Start engines, access doors open	1 min
Close access doors	1 min
Bring up power and set tunnel q and angles	4 min
For polar (time to set α and adjust power)	3-4 min/point
7-9 points/polar	~30 min
Reduce power and tunnel q	3 min
	≈ 35 min at power
Rotary wing	
V_∞ = 0 → 300 knots	
Time scenario, once operating conditions have been set	
Set vehicle operating conditions	4 min
Static and dynamic data	1 min
Flutter measurement and on-line data reduction	5 min
Test sequence, 5-10 points	25-50 min
	Desirable to have a minimum = 30 min

TABLE 2.- NUMERICAL VALUES FOR HEAT TRANSFER AND HEAT CAPACITY OF 40 × 80 TUNNEL STRUCTURE

Parameter	As determined by least-squares fit to data	As determined by graphical fit to data[a]
W_aC_p	0.432×10^6 Btu/°F	0.432×10^6 Btu/°F
W_sC_s	1.105×10^6 Btu/°F	$.596\times10^6$ Btu/°F
Sk/δ	376.8 Btu/sec/°F	391.1 Btu/sec/°F

[a]From Kenneth W. Mort, unpublished analysis, 1974.

TABLE 3.- FAN DRIVE TIME[a] AVAILABLE BEFORE TUNNEL TEMPERATURE RISES 50°F AS A FUNCTION OF AIR-EXCHANGE RATE

$\dot{m}$, %	Δt, min, no engine	Δt, min, one J97	Δt, min, two J97s
0	14.2	12.7	11.6
1	15.4	13.8	12.4
2	17.1	15.0	13.4
4	22.7	18.9	16.3
6	55.6	29.6	22.4
10	∞	∞	∞

[a]Times shown do not include time required to bring fan drive system to full power and to stabilize flow within 40 × 80 tunnel.

TABLE 4.- TIME ESTIMATES FOR COOLDOWN OF 40 × 80 TUNNEL USING AIR EXCHANGE: $T_i - T_o = 50°F$, ΔT_c = amount of cooldown of tunnel, $\dot{m} = 0.06$, P_c = power of tunnel set to cool tunnel

ΔT_c, °F	Δt = time required, min	
	$P_c = P_{max}/8$, equation (5)	P_c = optimum power, equation (12)
10	6.6	6.6
20	16.0	15.7
30	32.6	29.7
40	Not possible	56.9

TABLE 5.- INTAKE AND EXHAUST DATA ON FULL-SCALE FACILITY 1982 IST: OLD LOUVERED AIR INLET, THREE DOORS REMOVED FROM SOUTH END

Run No.	Inlet No./ court-yard, ft^2	Exhaust area, ft^2	$\frac{p_s-H_{atm}}{q_{ts}}$	$\frac{H_s-H_{atm}}{q_{ts}}$	% air exchanged through south wall doors	$\frac{H_{atm}-p_n}{q_{ts}}$	% air exchanged by north leg pressure	% air exchanged through courtyard exhaust	$\frac{p_s-p_n}{q_{ts}}$	Total flow rate, %
64	401/0	562	+0.040	+0.058	3.0	-0.193	3.0	0	0.233	3
65	0/0	562	+.005	+.019	~1.0	-.235	--	0	.240	~1
66	401/401	562	+.091	+.105	4.6	-.150	2.3×2	0	.241	4.6
67	401/401	1170[a]	+.068	+.082	3.9	-.170	2.6×2	1.3	.238	5.2
68	401/0	1170[a]	+.025	+.039	2.5	-.212	3.2	.7	.237	3.2

[a]Area includes two screened openings in south leg of facility near midpoints of courtyard and south walls.

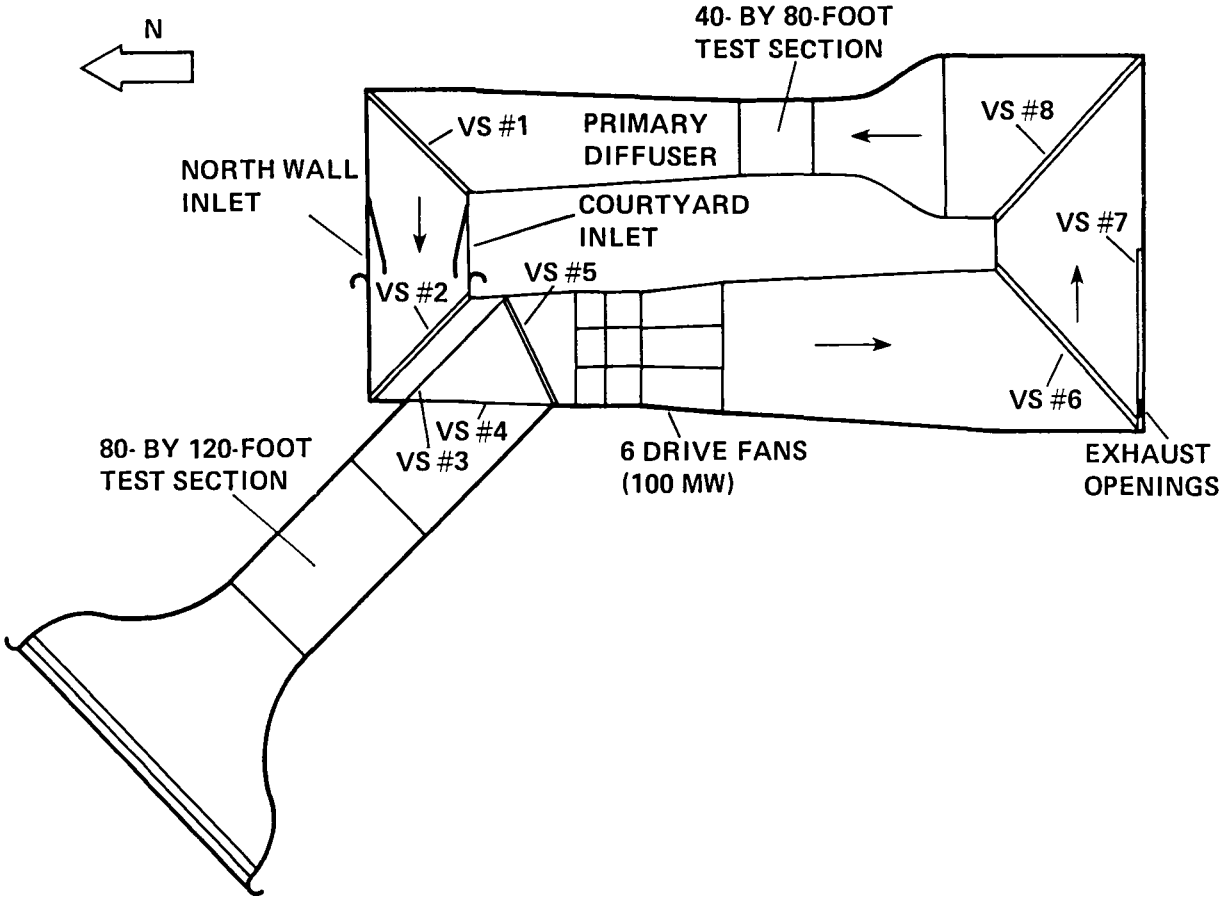

Figure 1.- Diagram of plan view of the National Full-Scale Aerodynamics Complex (NFAC) at NASA Ames Research Center which illustrates the 40- by 80-ft and 80- by 120-ft tunnel circuits.

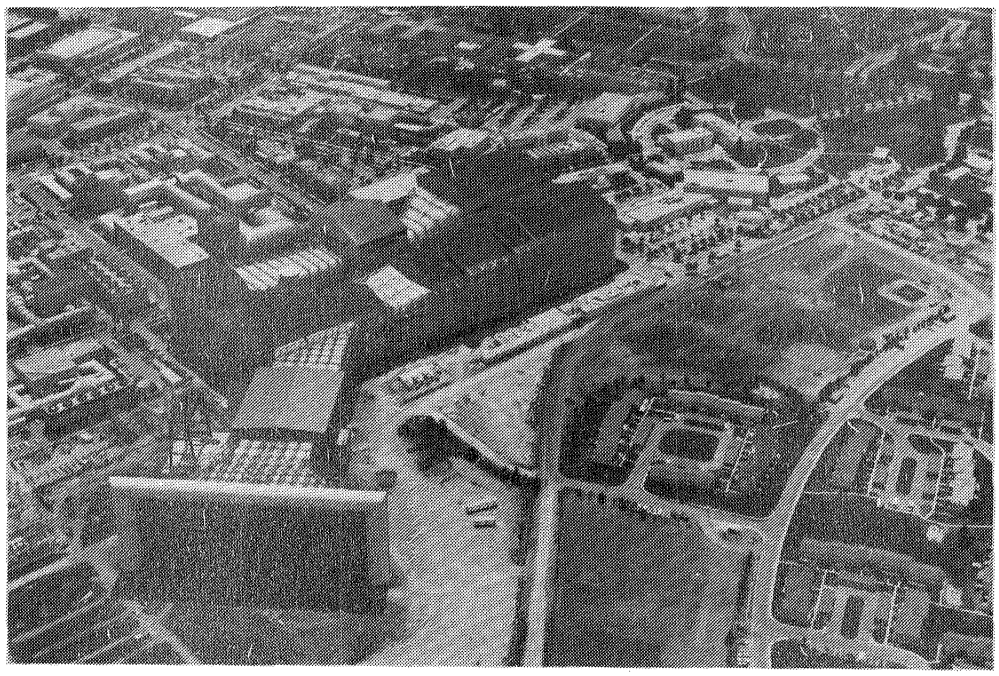

(a) View of facility looking into the entrance of the 80 × 120 tunnel from the northwest.

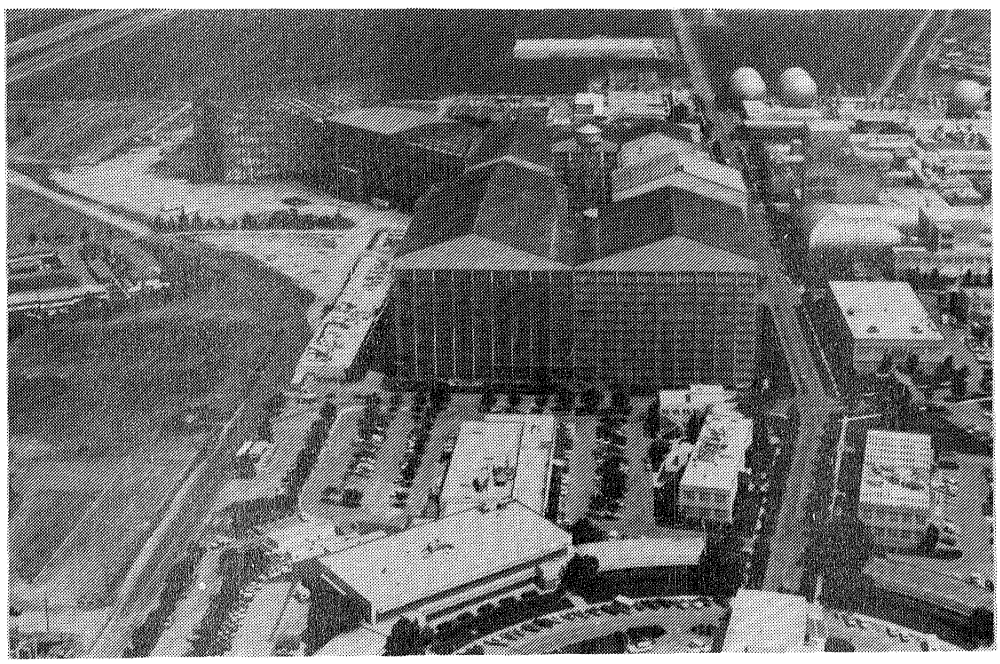

(b) View of facility looking at south wall of 40 × 80 tunnel circuit.

Figure 2.- NFAC showing both the circuit of the 40 × 80 tunnel and of the 80 × 120 tunnel and surrounding buildings.

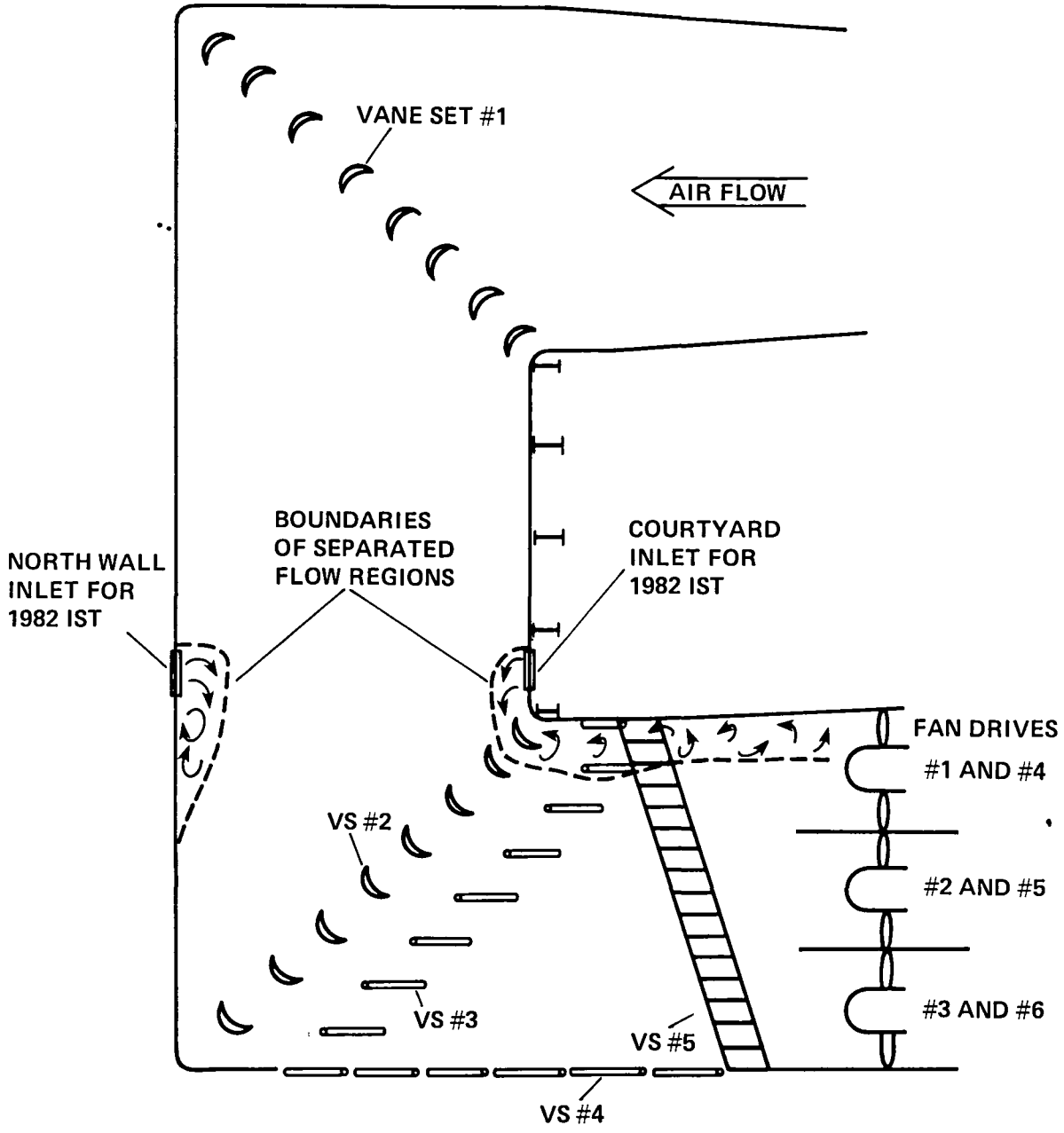

Figure 3.- Diagram of northern part of the 40 × 80 tunnel circuit illustrating separated flow regions instigated by inflow through louvered air-exchanger inlets used during 1982 IST.

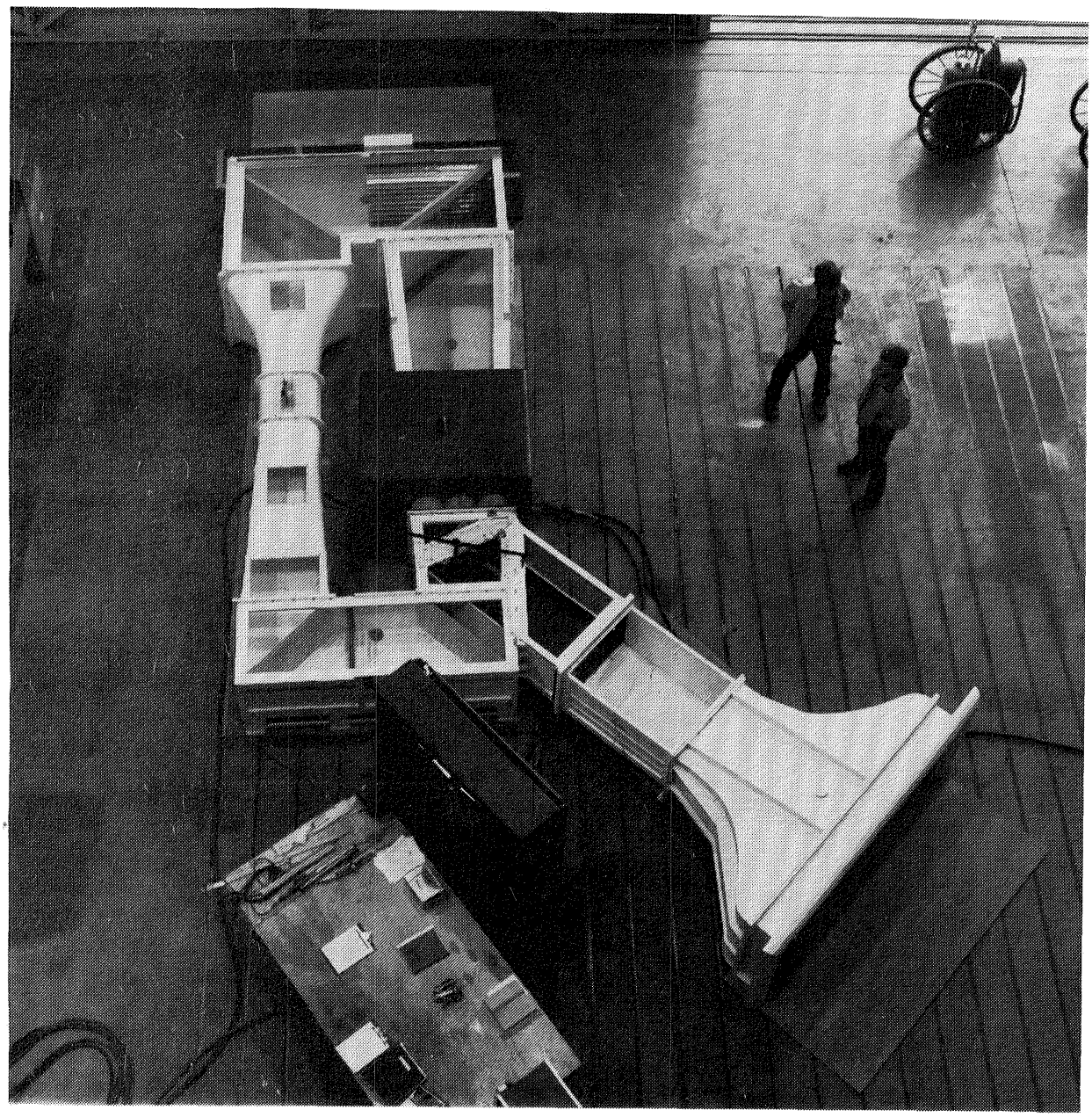

Figure 4.- One-fiftieth-scale model of NFAC used in the present experimental investigation.

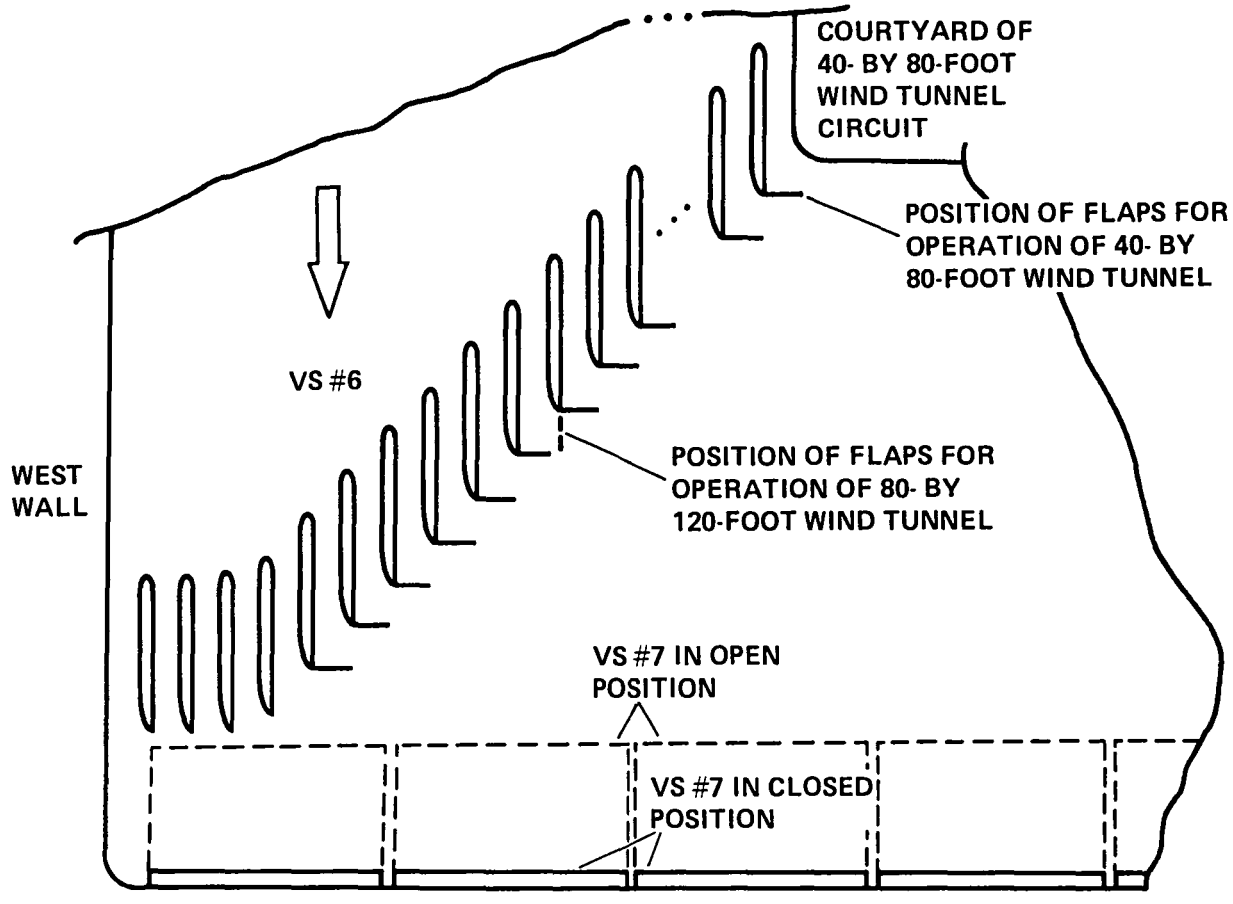

Figure 5.- Plan view of southwest corner of NFAC, illustrating offset of three corner vanes and removal of four flaps from vane set No. 6 (which contains a total of 57 vanes) to accommodate the inward swing of vane set No. 7 as it opens for 80 × 120 tunnel operation. Debris screen and structure on outside of building are not shown.

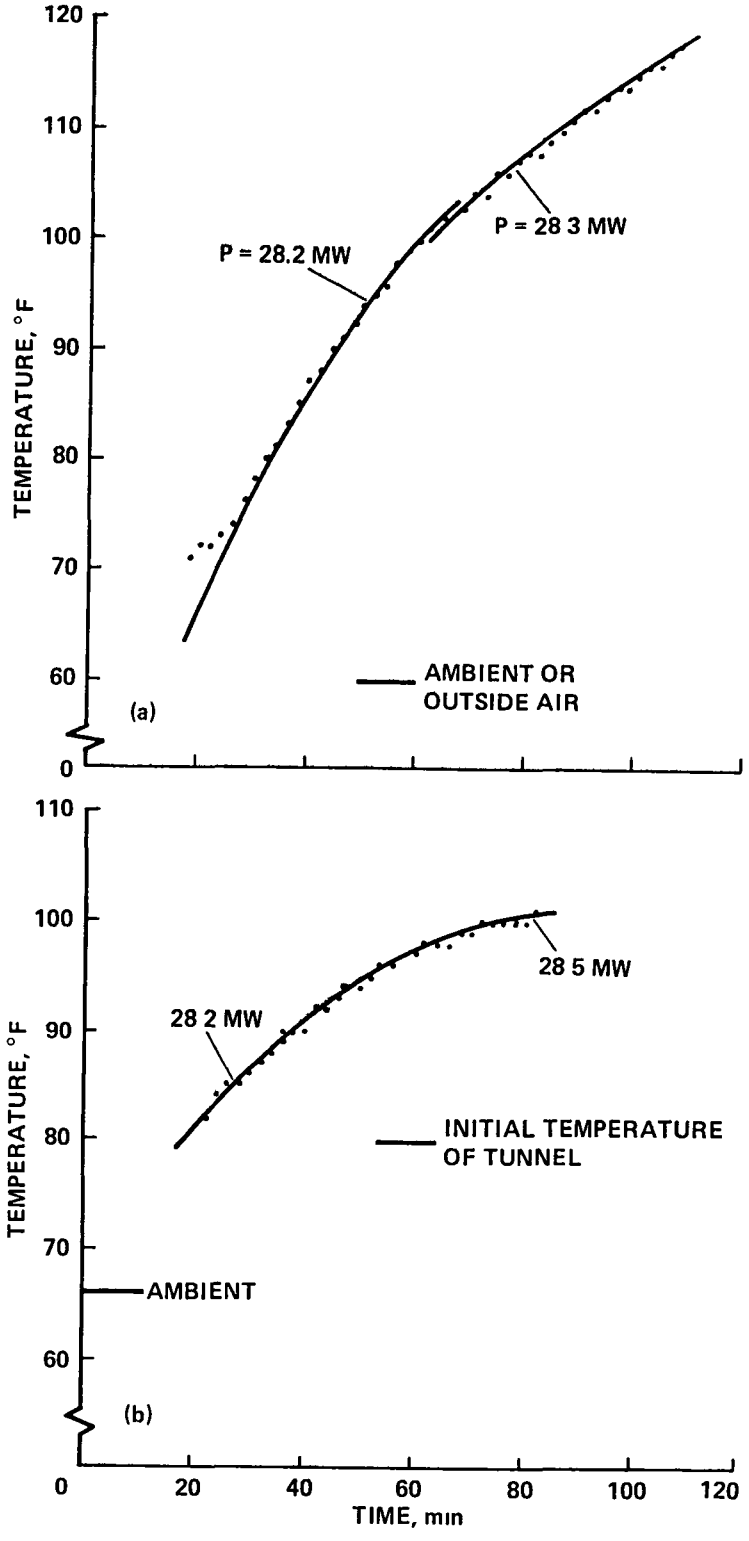

Figure 6.- Temperature-time data from full-scale facility that was used to determine thermal constants in heat equation. (a) Test 446, run 1: Ambient temperature = initial tunnel temperature = 60°F; louvers and roll doors closed ($\dot{m} \approx 0$); q_{ts} = 120 lb/ft^2. (b) Test 446, run 2: Ambient temperature = 66°F; initial tunnel temperature = 80°F; louvers and roll doors open; $q_{ts} \approx$ 118 lb/ft^2.

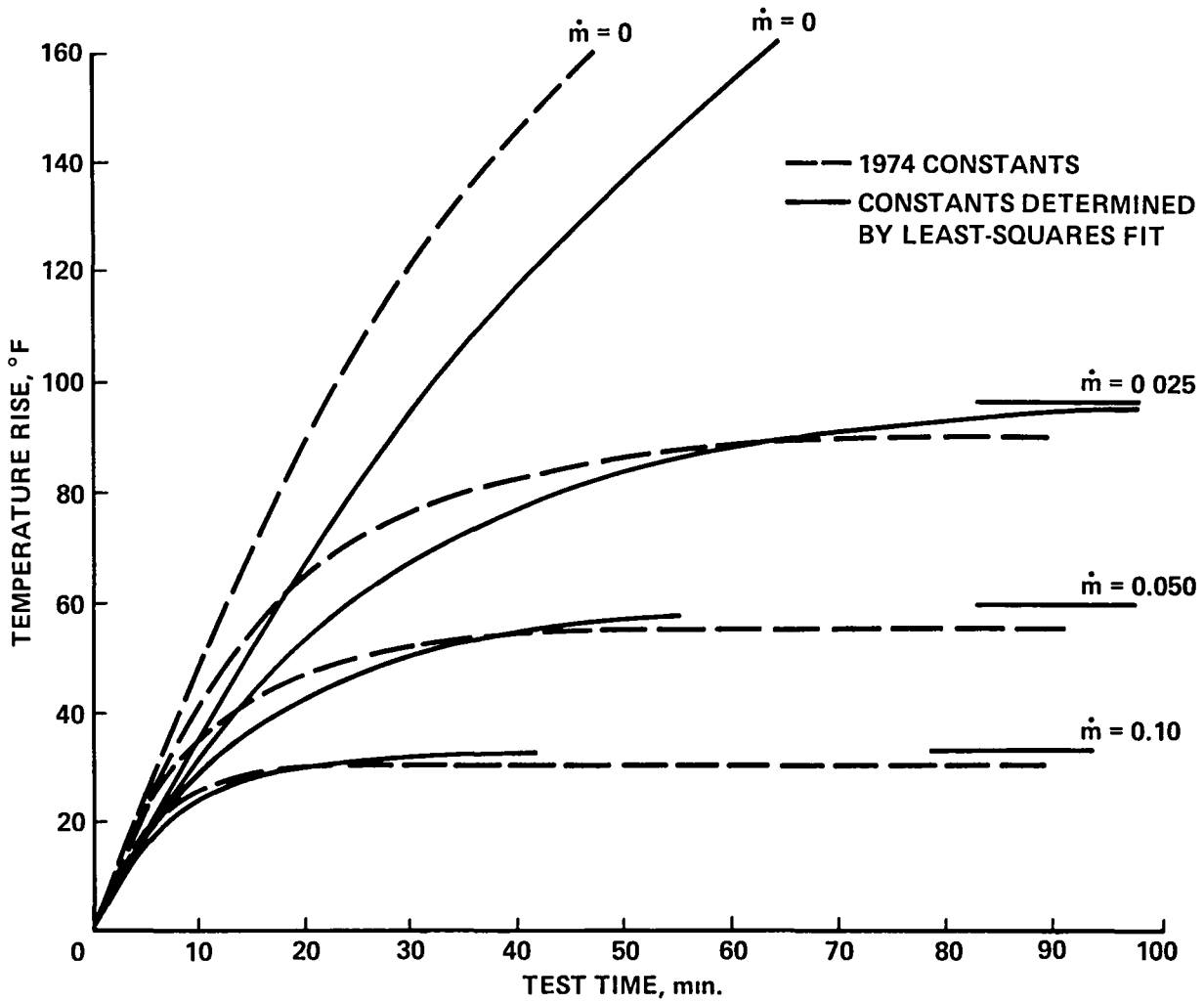

Figure 7.- Comparison of heating curves from two sets of constants.

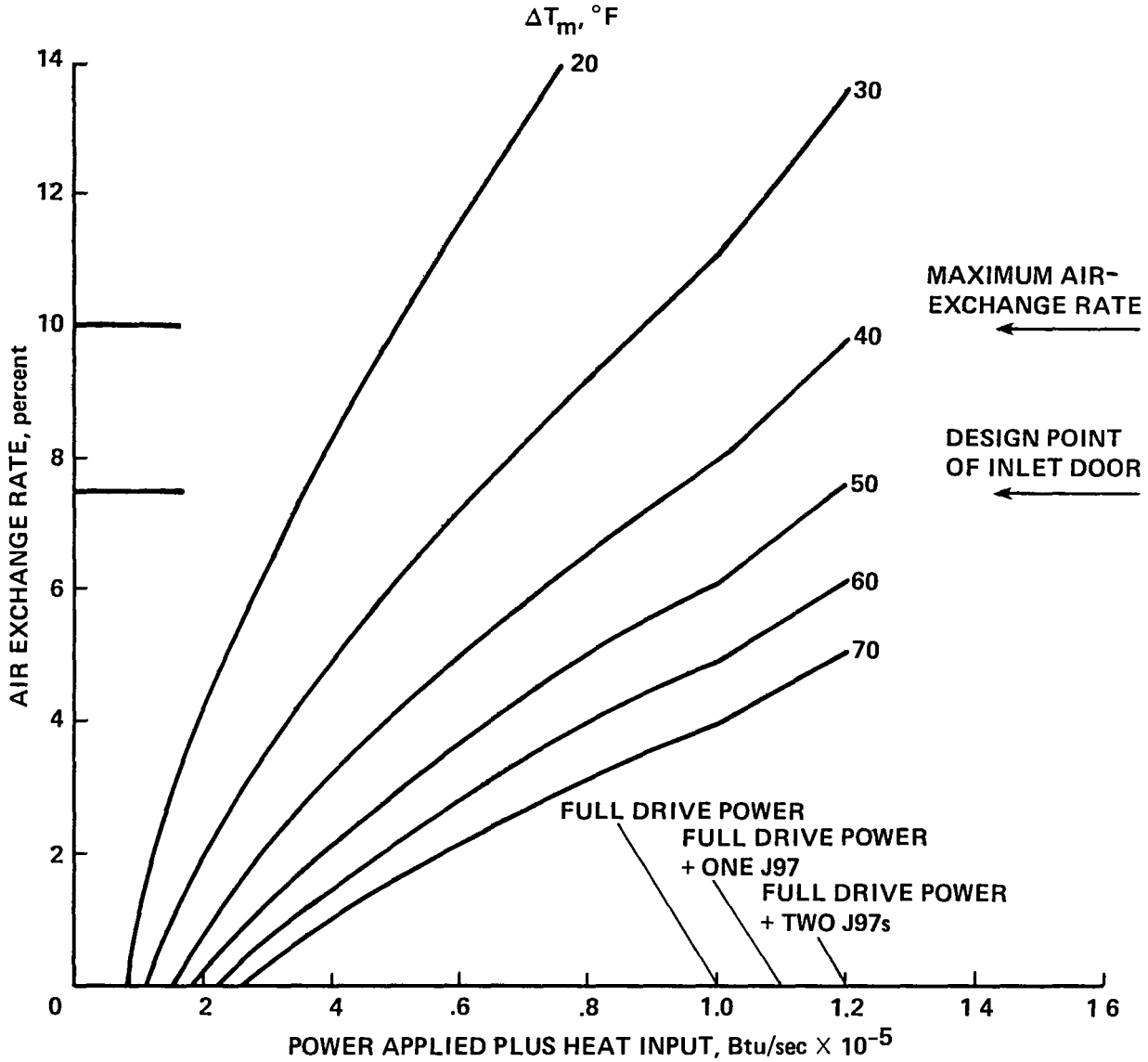

Figure 8.- Effect of applied drive power and engine heat on air-exchange rate required to maintain a given air temperature in 40 × 80 tunnel circuit.

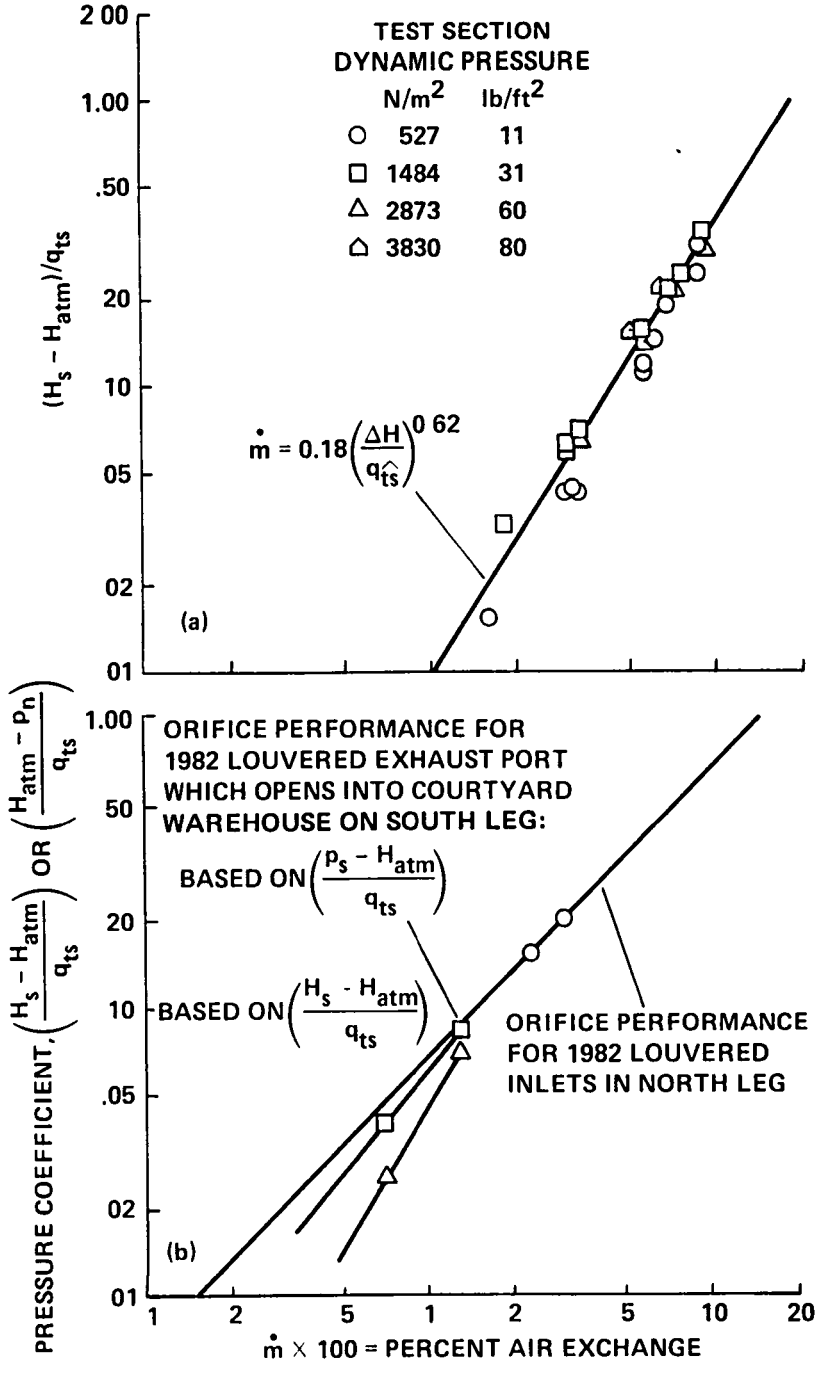

Figure 9.- Measured air-exchange rates for a range of pressure differences across the walls to calibrate orifices; three wall panels removed for exhaust area in south wall. (a) Exhaust orifices in south leg of 40 × 80 tunnel; inlet for air is of contoured-door type. (b) Inlet orifices in north leg of facility and courtyard exhaust orifice.

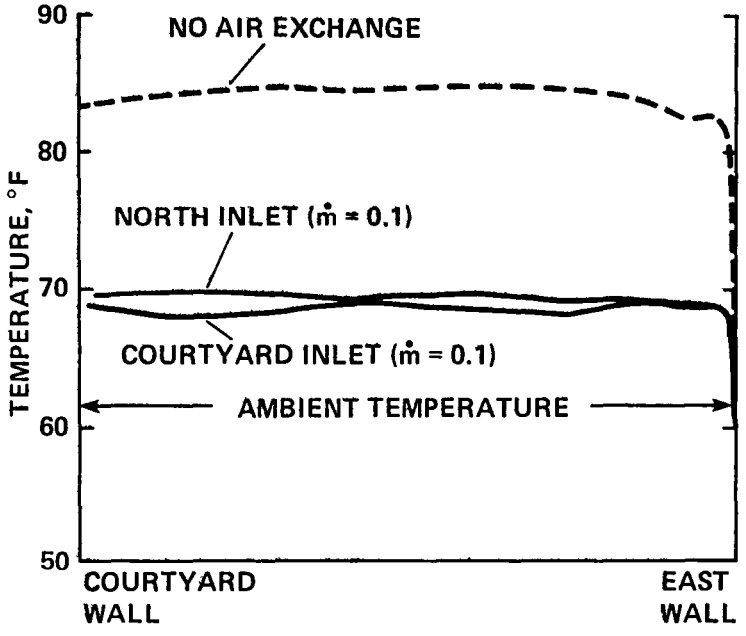

Figure 10.- Temperature profiles across test section through centerline of tunnel; $q_{ts} \approx 57$ lb/ft^2.

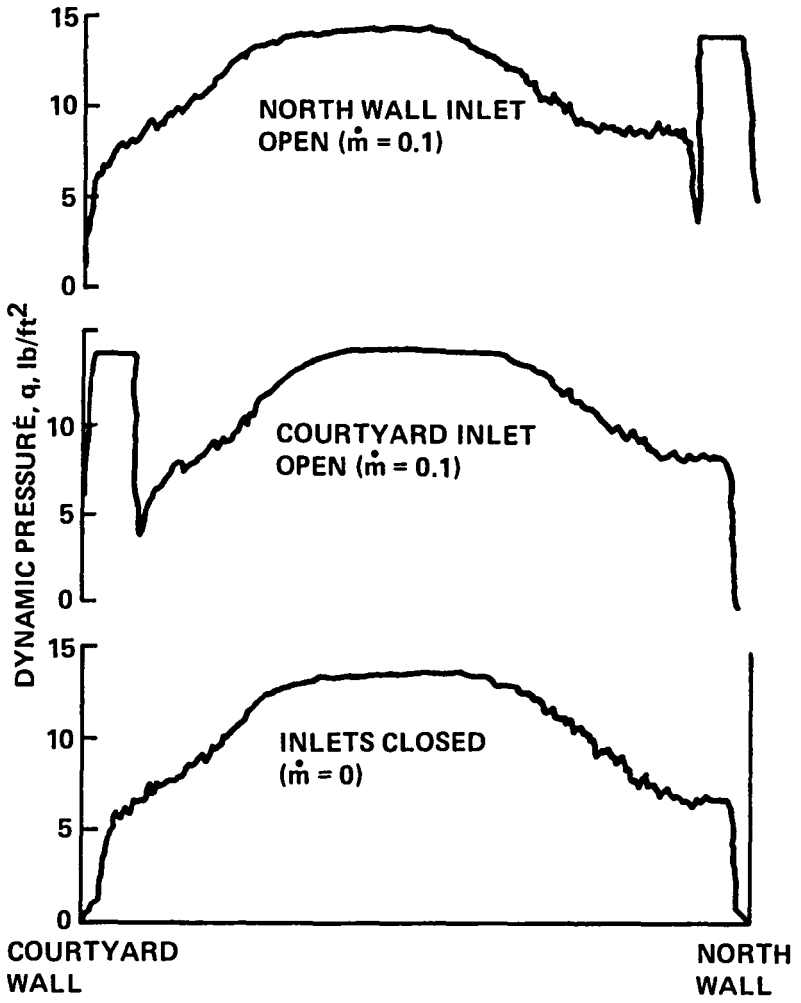

Figure 11.- Profiles of dynamic pressure across tunnel on horizontal plane through centerline of tunnel 1 in. downstream of inlets; $q_{ts} \approx 57$ lb/ft^2. No screens or superstructure over proposed contoured inlets. Records are offset to clarify changes in curve shapes.

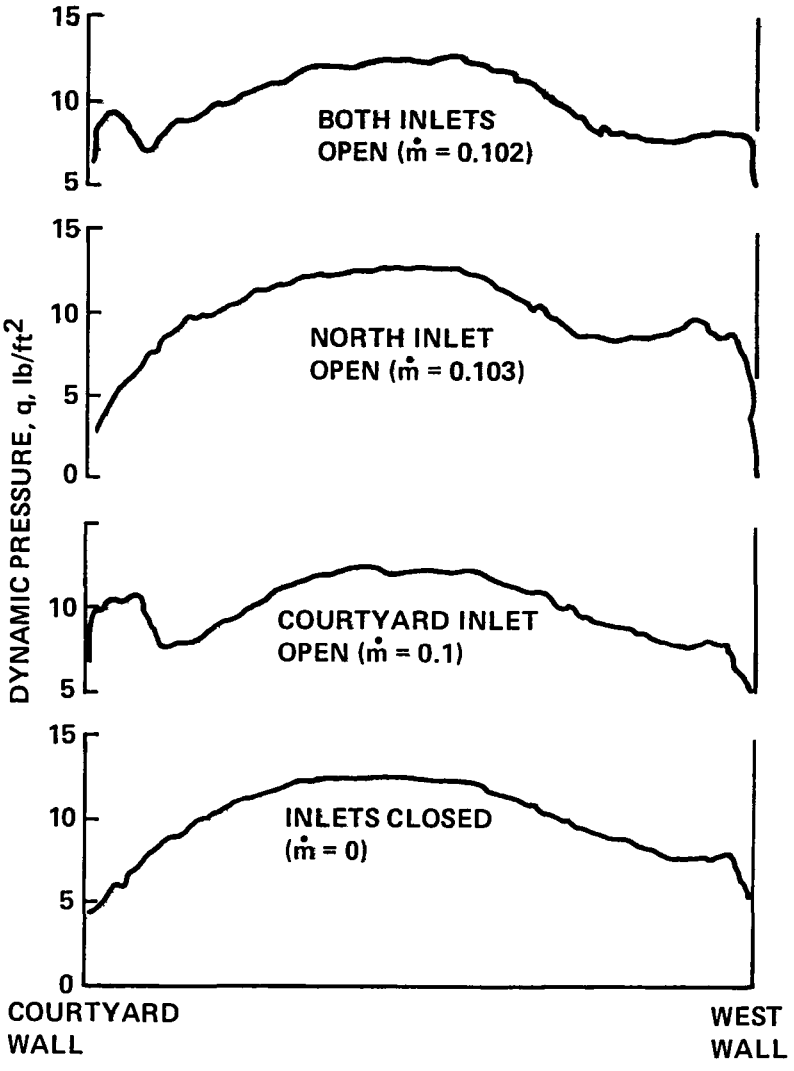

Figure 12.- Profiles of dynamic pressure across tunnel on horizontal plane through centerline of tunnel just upstream of vane set No. 5; $q_{ts} \approx 56$ lb/ft^2.

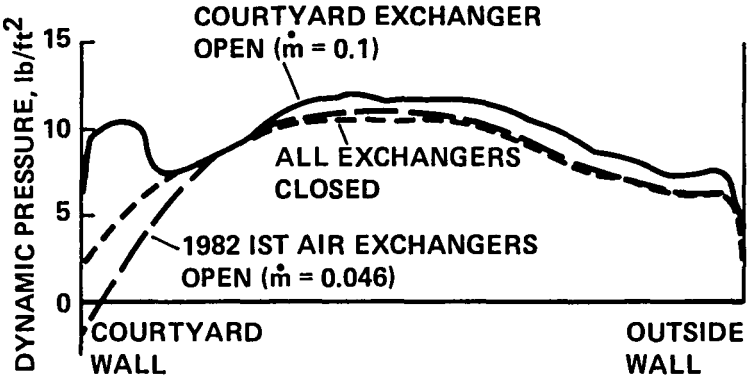

Figure 13.- Variation of dynamic pressure across wind-tunnel channel just upstream of vane set No. 5 for three air-exchange configurations.

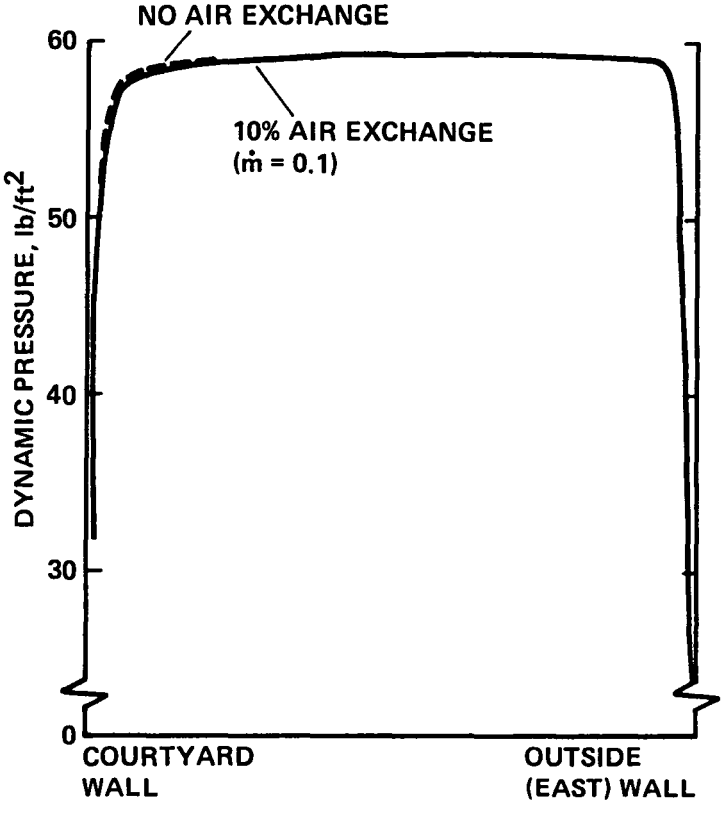

Figure 14.- Profiles of dynamic pressure across test section through centerline of tunnel with and without air exchange; $q_{ts} \approx 59$ lb/ft^2.

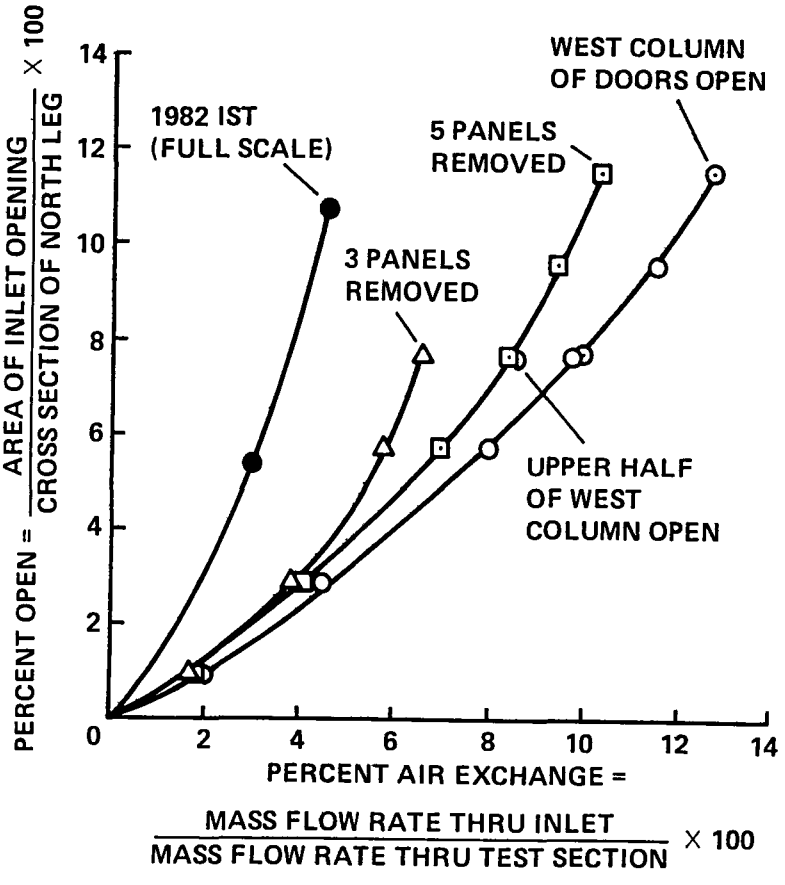

Figure 15.- Opening of courtyard inlet required to obtain a given air-exchange rate for several exhaust configurations (open symbols denote 1/50-scale data).

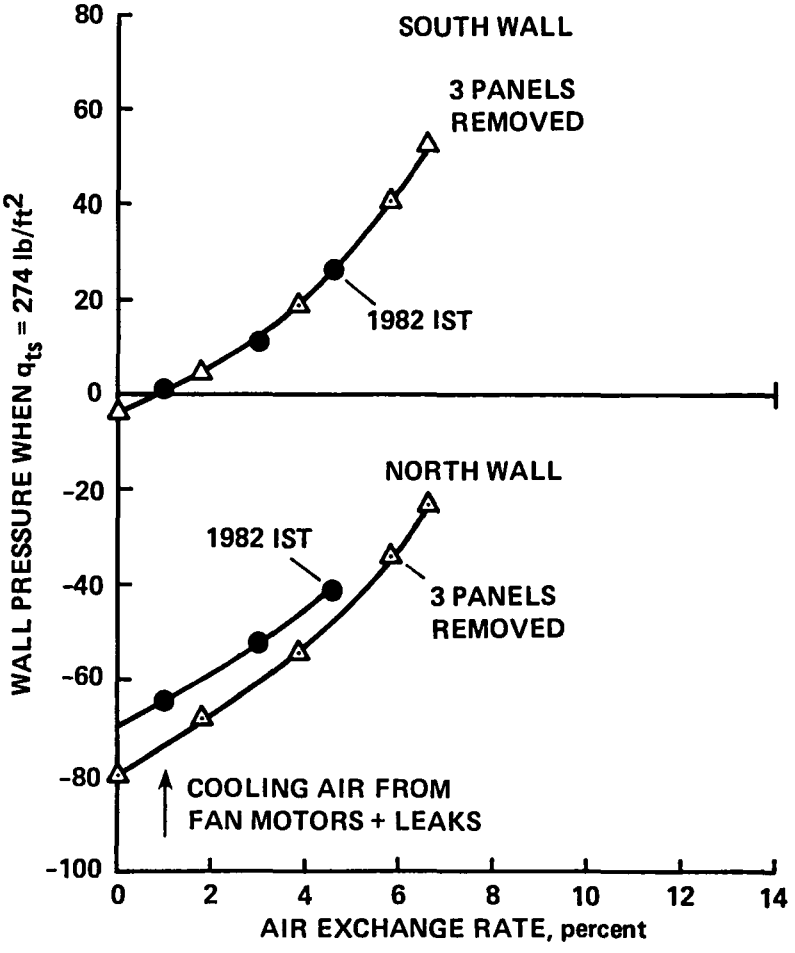

Figure 16.- Pressure difference across north and south walls of 40 × 80 tunnel at maximum design velocity (q_{ts} = 274 lb/ft^2); comparison of data from 1/50-scale model, using courtyard inlet with full-scale data taken during 1982 IST.

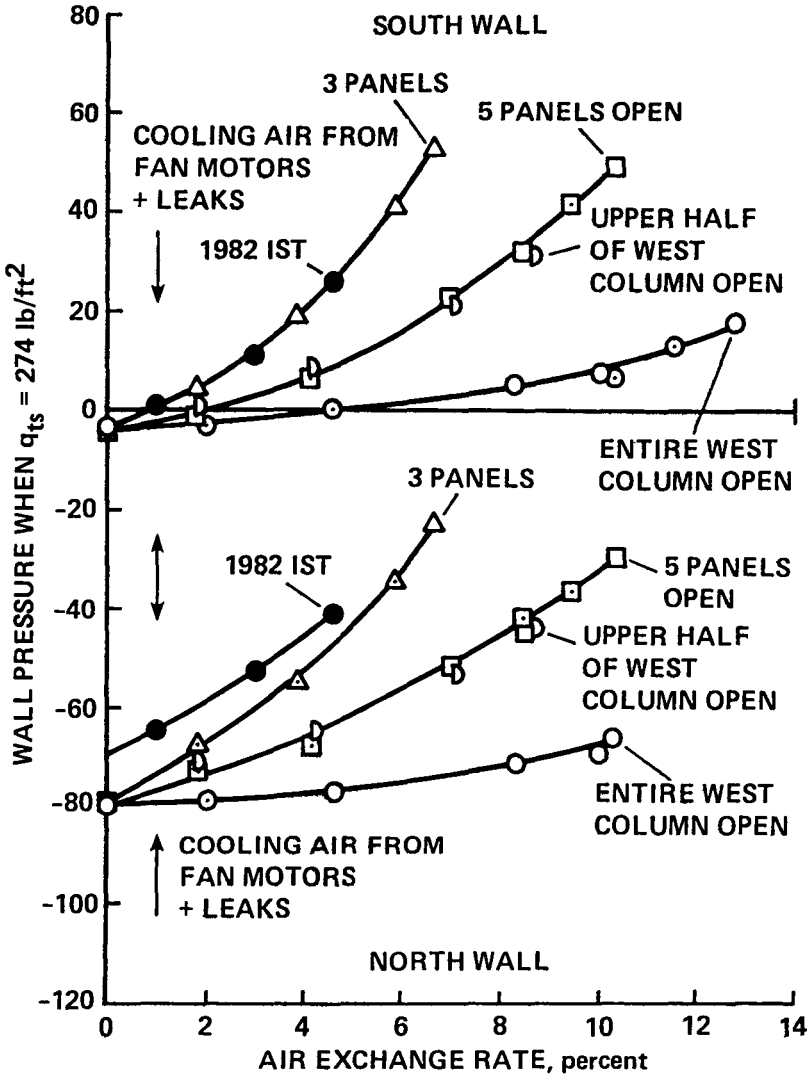

Figure 17.- Pressure difference across north and south walls of 40 × 80 tunnel for various exhaust configurations, using only the courtyard inlet as a function of percent air exchange. Data from full-scale IST (solid symbols) and from 1/50-scale model (open symbols) have been interpreted at the maximum dynamic pressure of q_{ts} = 274 lb/ft^2.

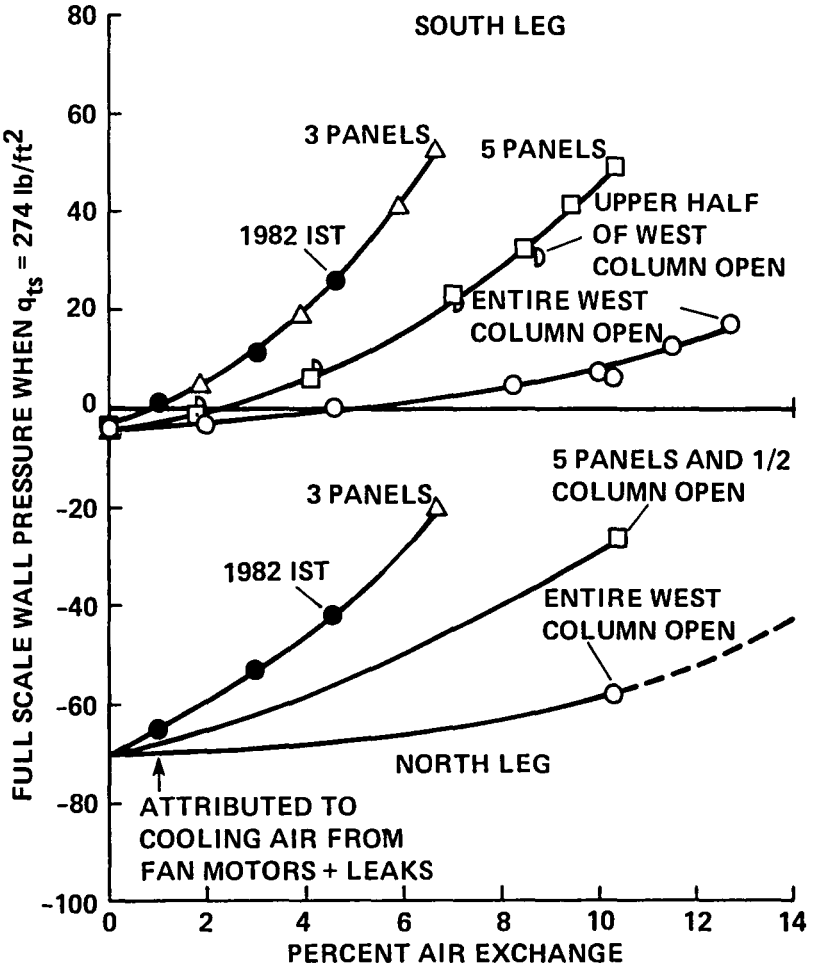

Figure 18.- Pressure difference across walls of north and south legs of 40 × 80 tunnel for several exhaust configurations as a function of air-exchange rate. Only the courtyard inlet is used. Data obtained from 1982 IST and from 1/50-scale model. All data were first scaled to a test-section dynamic pressure of q_{ts} = 274 lb/ft^2 (300 knots). The north leg pressures were then adjusted by a factor of 7/8 to bring 1/50-scale model data in line with full-scale data.

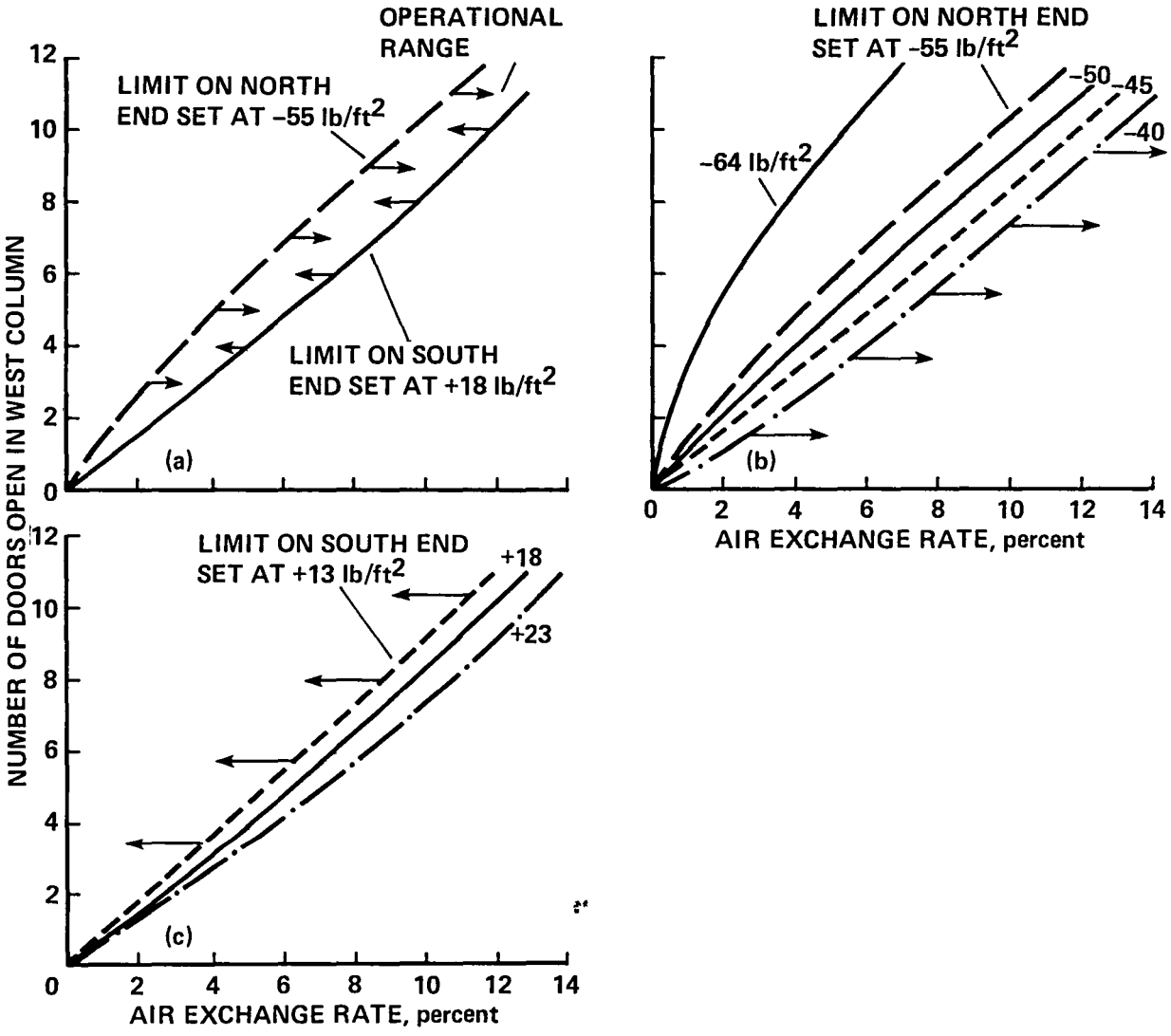

Figure 19.- Air-exchange rate required to keep wall pressures within specified limits when a given number of exhaust panels are open; q_{ts} = 274 lb/ft^2. Curves based on data from 1/50-scale model. (a) Sample case of -55 and +18 lb/ft^2. (b) Variation with pressure limit on north leg. (c) Variation with pressure limit on south leg.

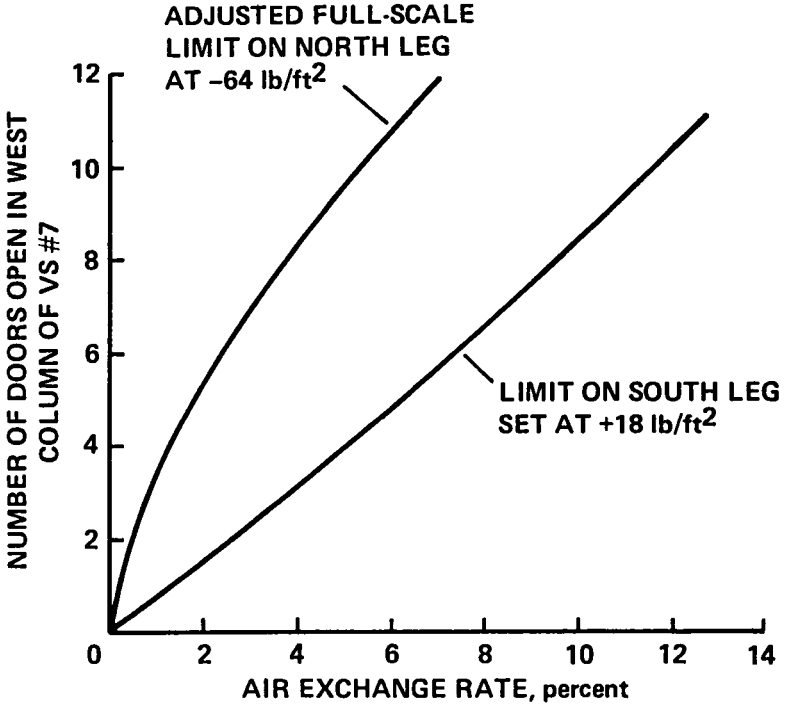

Figure 20.- Allowable air-exchange rates for 40 × 80 tunnel circuit when limits are set on north leg at -64 lb/ft^2 (-74 lb/ft^2 in model) and on south leg at +18 lb/ft^2.

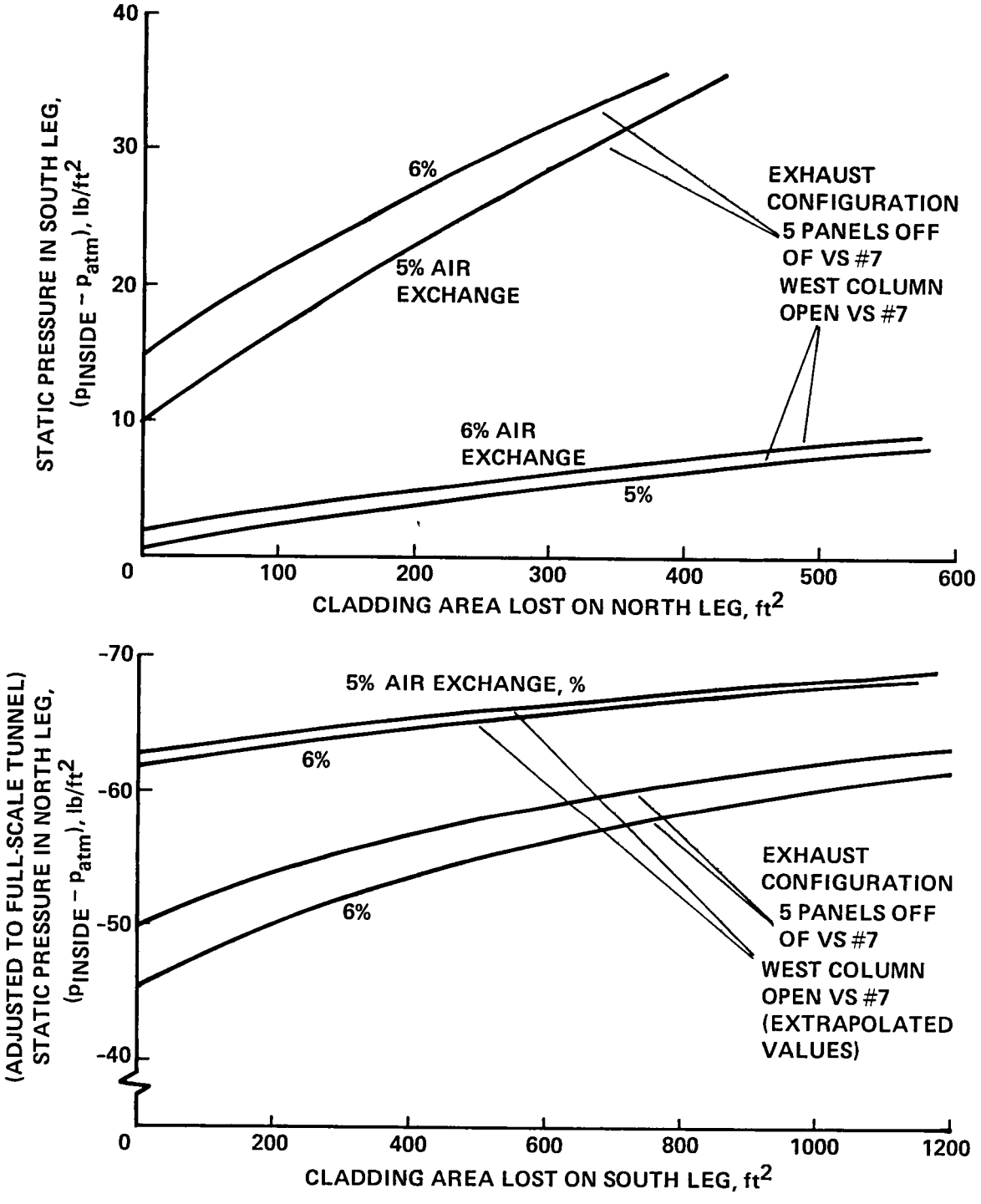

Figure 21.- Pressure changes to be expected in 40 x 80 tunnel circuit if cladding is lost at maximum tunnel speed and approximately 5% and 6% air exchange, at maximum power.

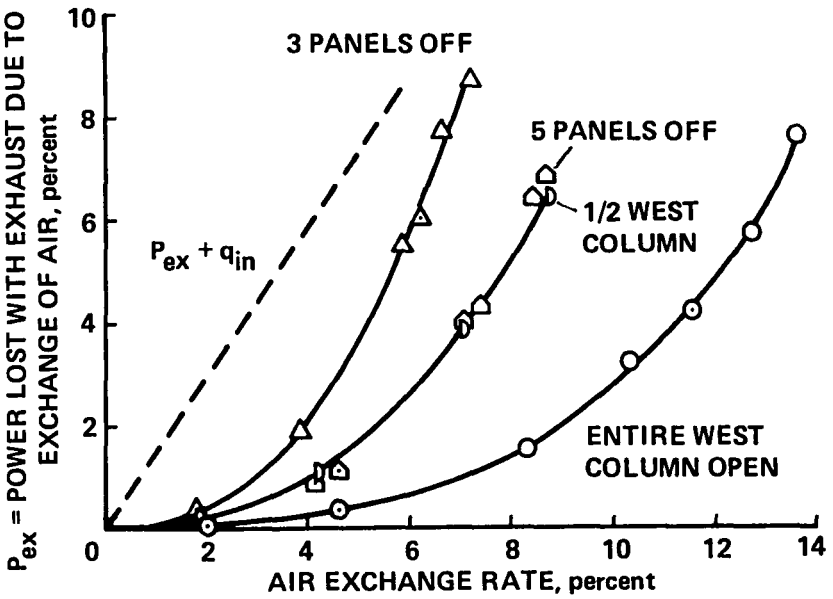

Figure 22.- Comparison of power required to drive air exchange for various exhaust configurations when inlet is of courtyard-door type.

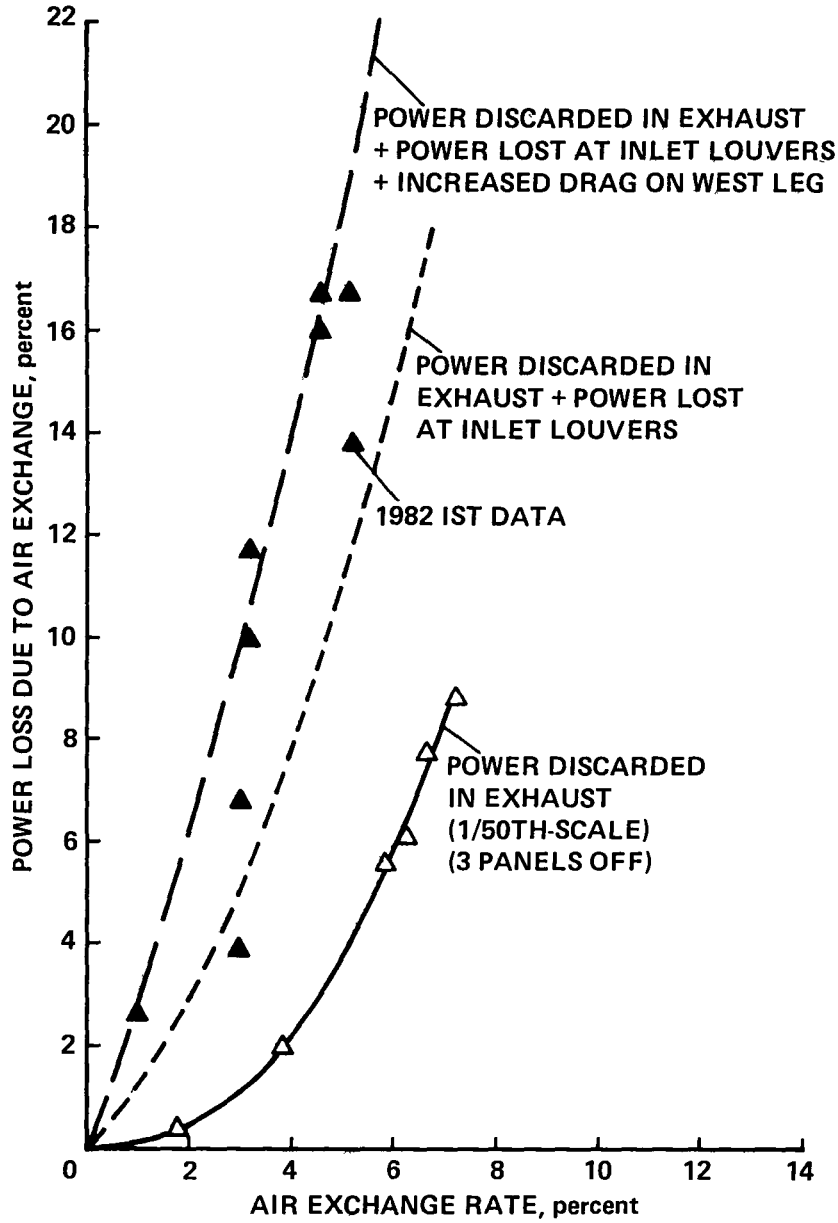

Figure 23.- Contributions to power loss for air exchange for old louvered inlet and three-panels off exhaust and comparison with 1982 IST data.

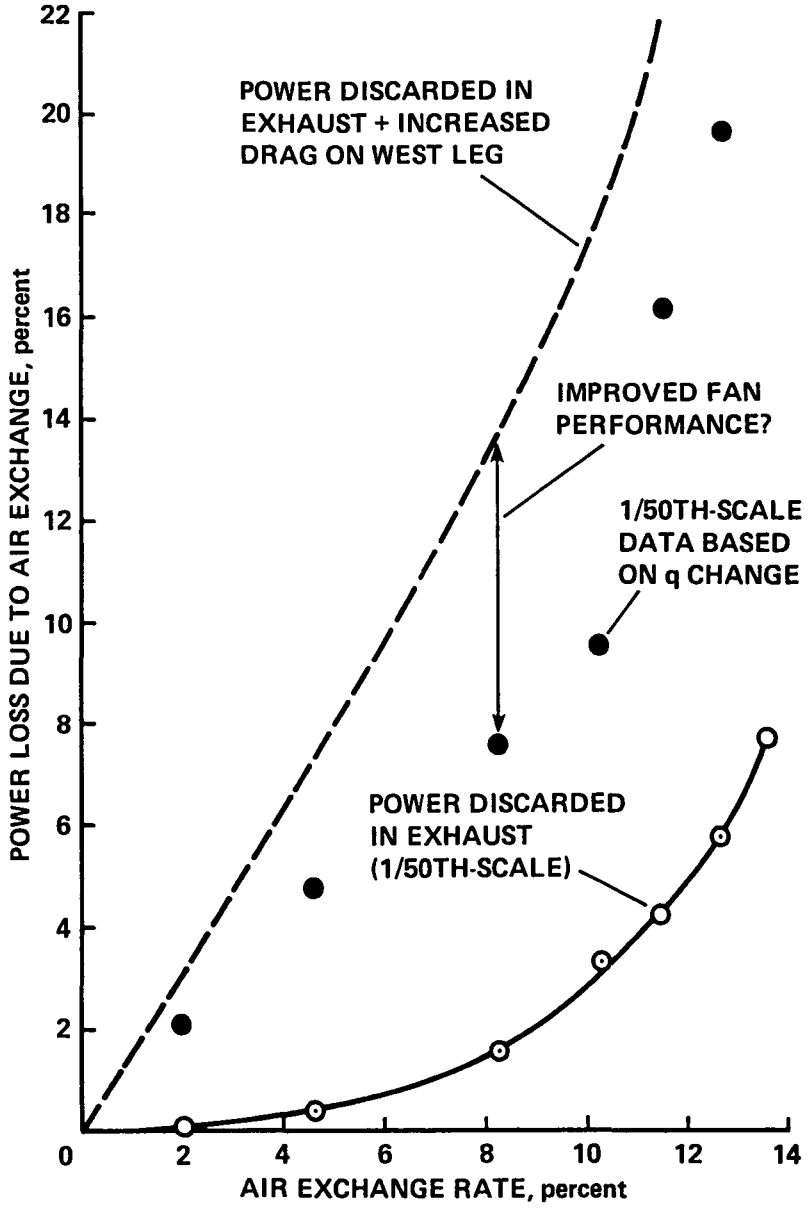

Figure 24.- Contributions to power loss for door-type inlet and entire west column of exhaust doors open; no bird screen or superstructure over inlet.

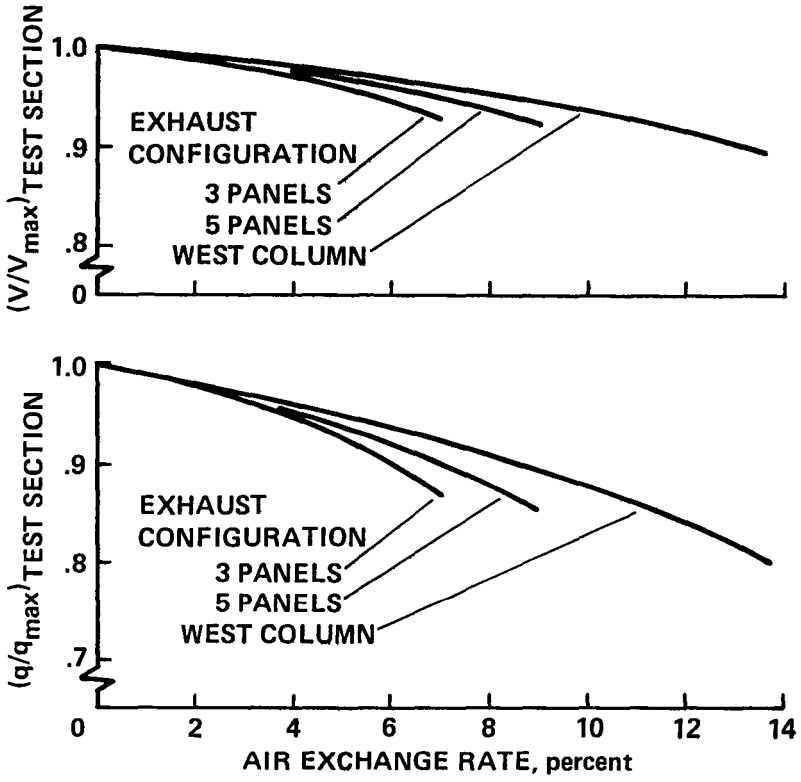

Figure 25.- Effect of air-exchange rate on maximum velocity and dynamic pressure capability of 40 × 80 tunnel for several exhaust openings (assumes V_{max} = 300 knots at 0% air exchange).

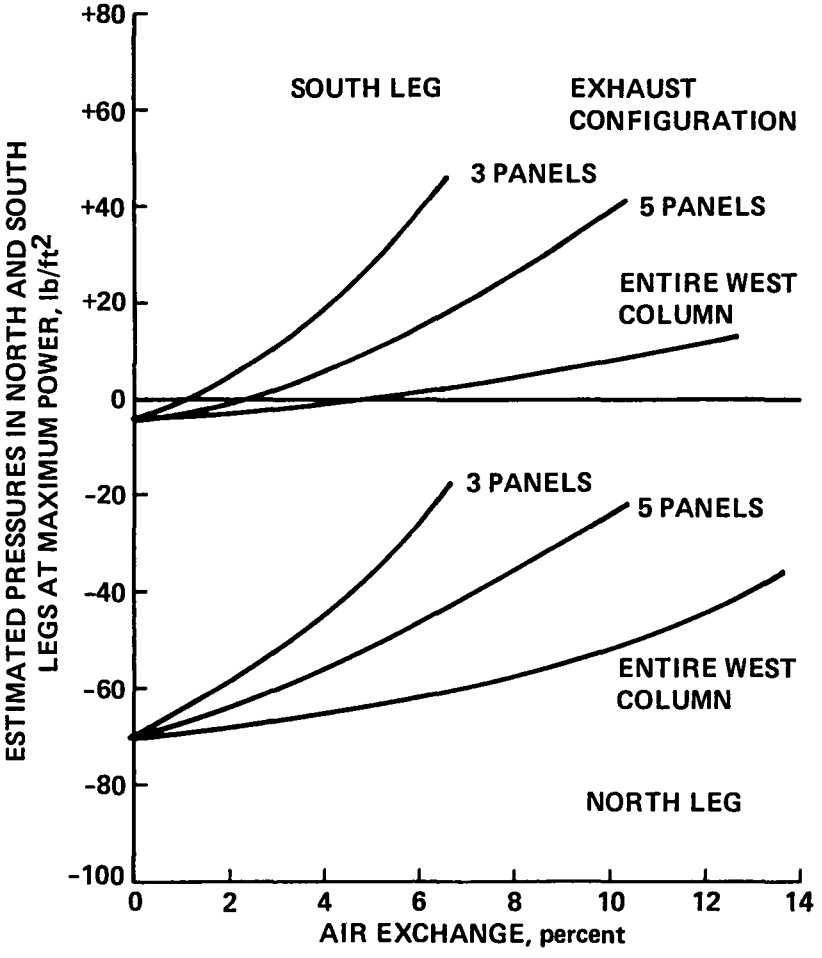

Figure 26.- Estimated pressure across walls of north and south legs of 40 × 80 tunnel at full power for several exhaust configurations. Data from 1/50-scale model adjusted to full-scale and corrected for power loss caused by air exchange.

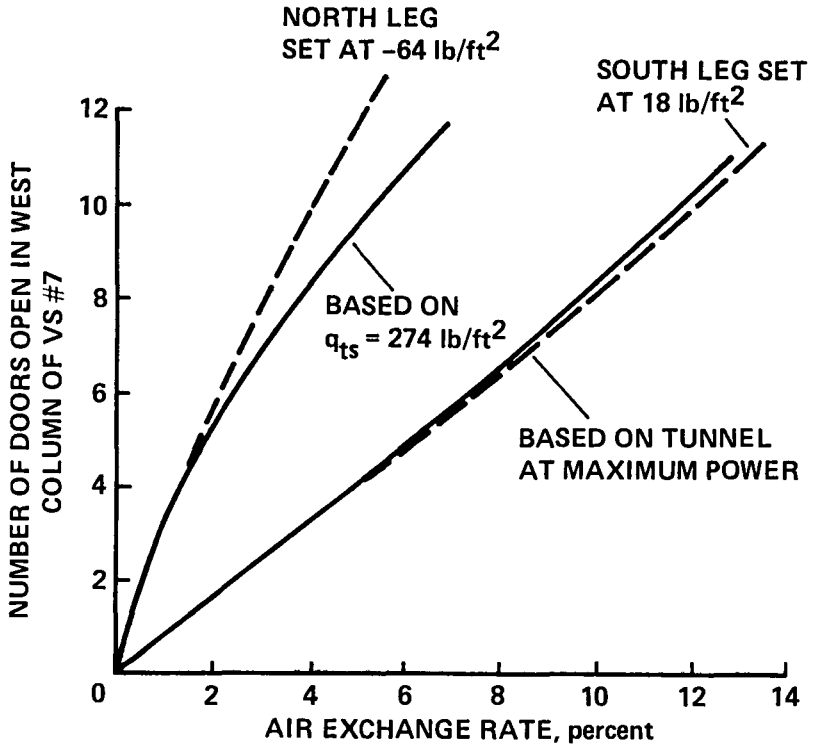

Figure 27.- Allowable air-exchange rates for 40 × 80 tunnel circuit when limits are set on north leg at -64 lb/ft^2 and on south leg at 18 lb/ft^2; comparison of results when tunnel is operated at q_{ts} = 274 lb/ft^2 with tunnel operated at full power.

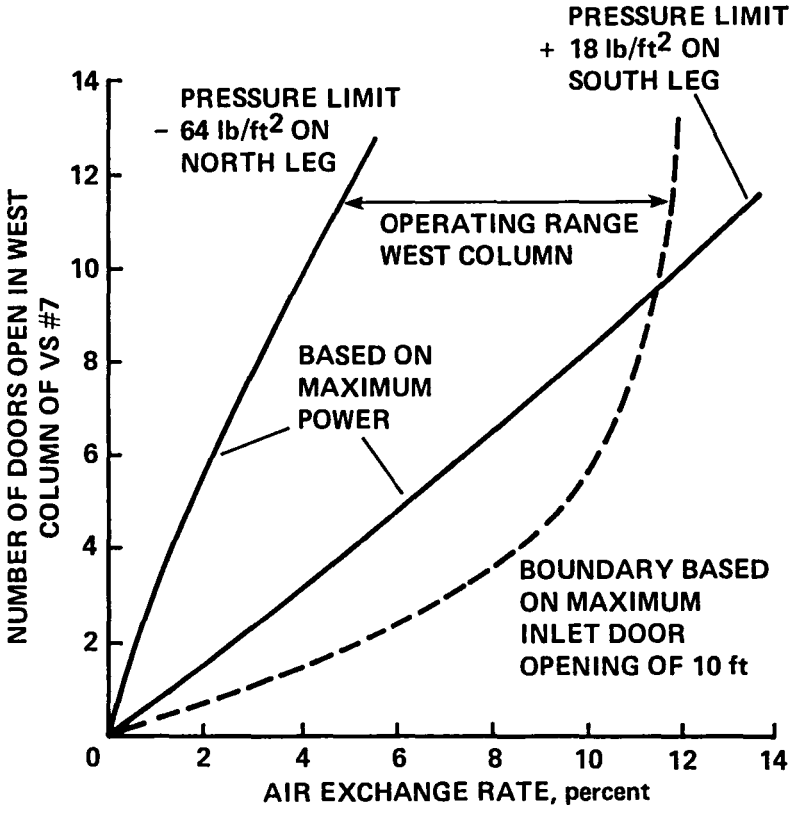

Figure 28.- Achievable air-exchange rates in 40 × 80 tunnel circuit at maximum power (assumes q_{ts} = 274 lb/ft^2 at 0% air exchange).

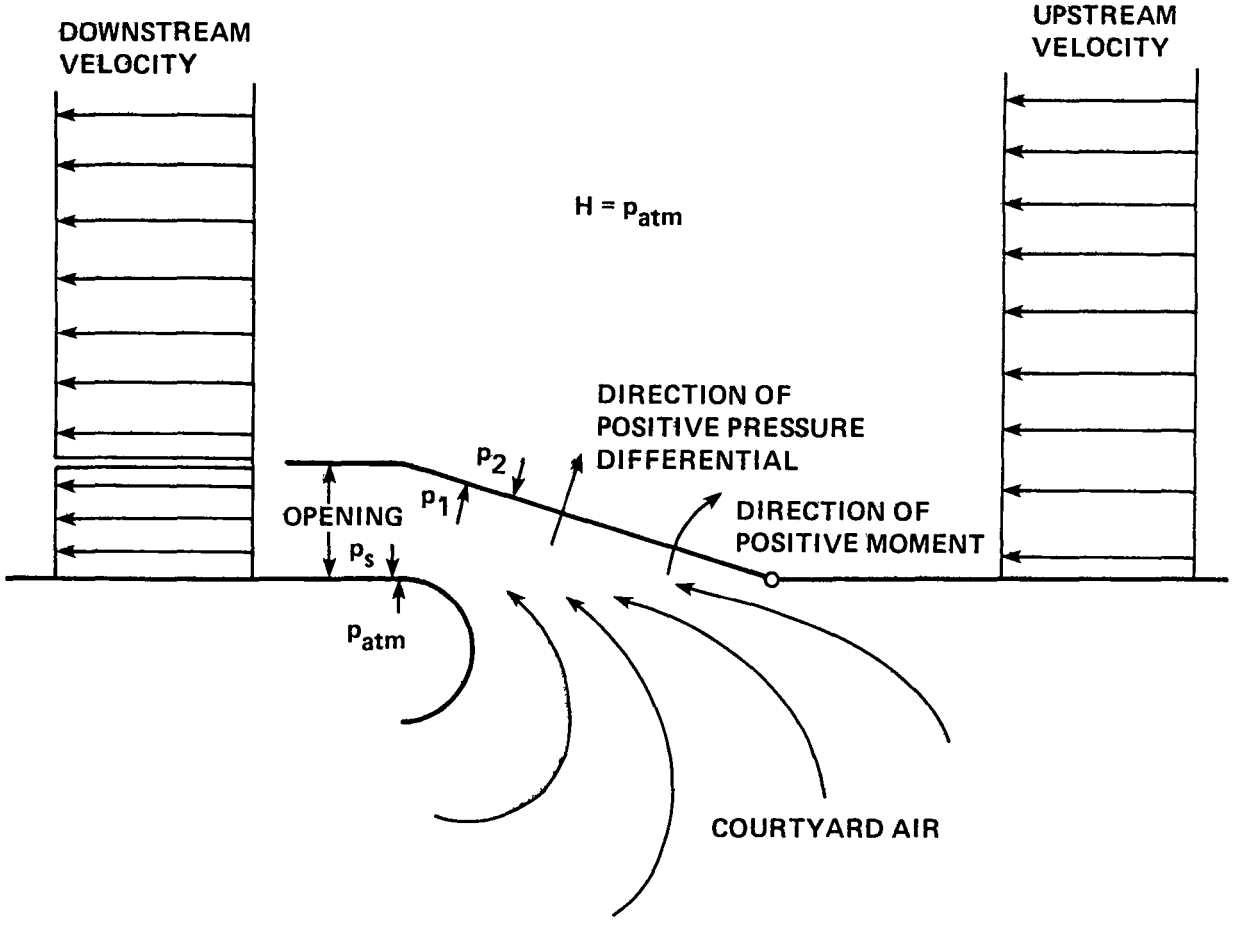

Figure 29.- Idealized model of flow field around inlet door as assumed in potential flow code.

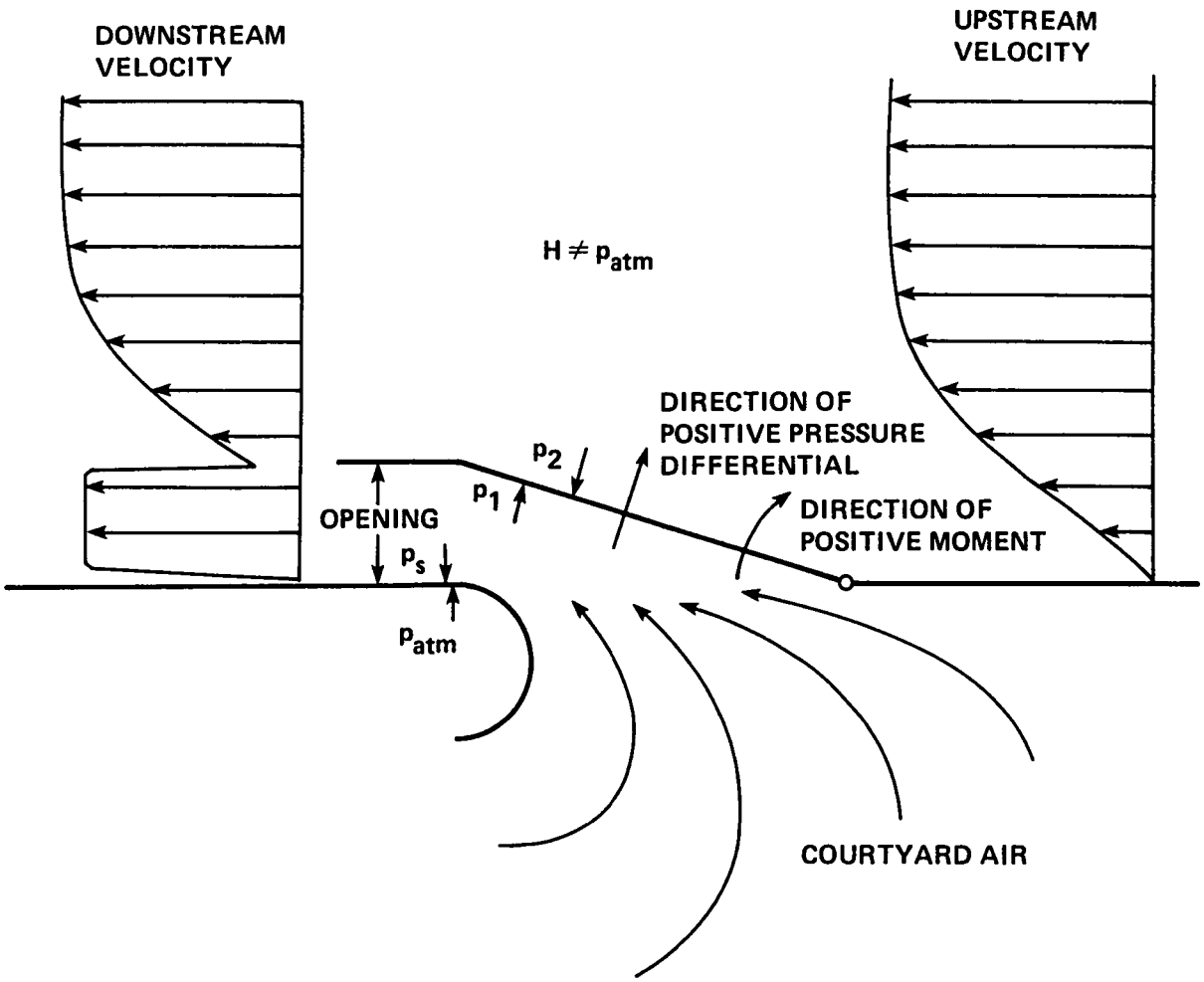

Figure 30.- Sketch of actual flow field in tunnel near air-exchanger inlet door.

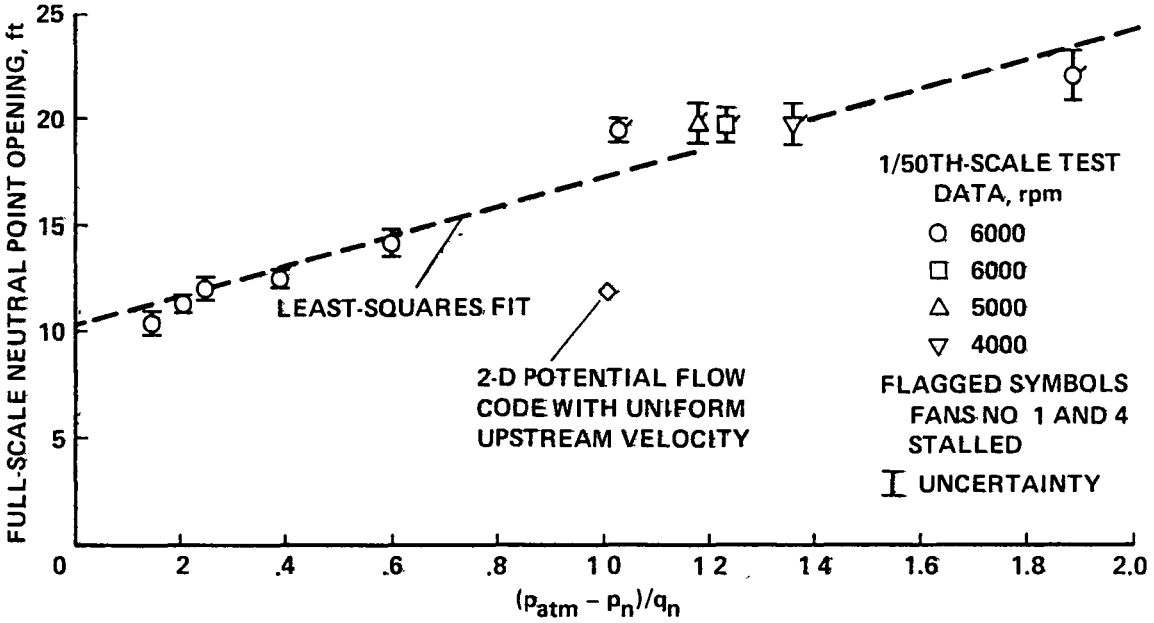

Figure 31.- Position of inlet door when permitted to swing freely, as if no hinge moment (neutral point), for various wind tunnel operating conditions.

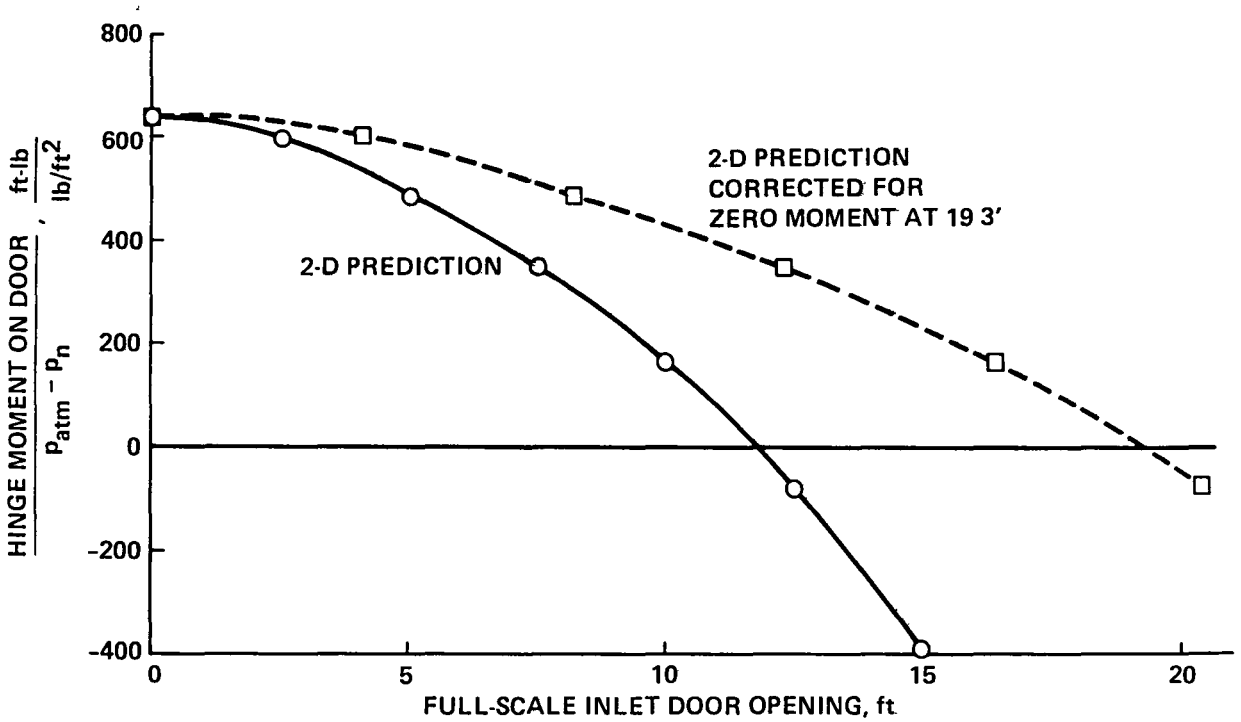

Figure 32.- Predicted and adjusted hinge moment on inlet door as a function of door opening; estimates are based on data from 1/50-scale model of tunnel; p_n = -64 lb/ft^2.

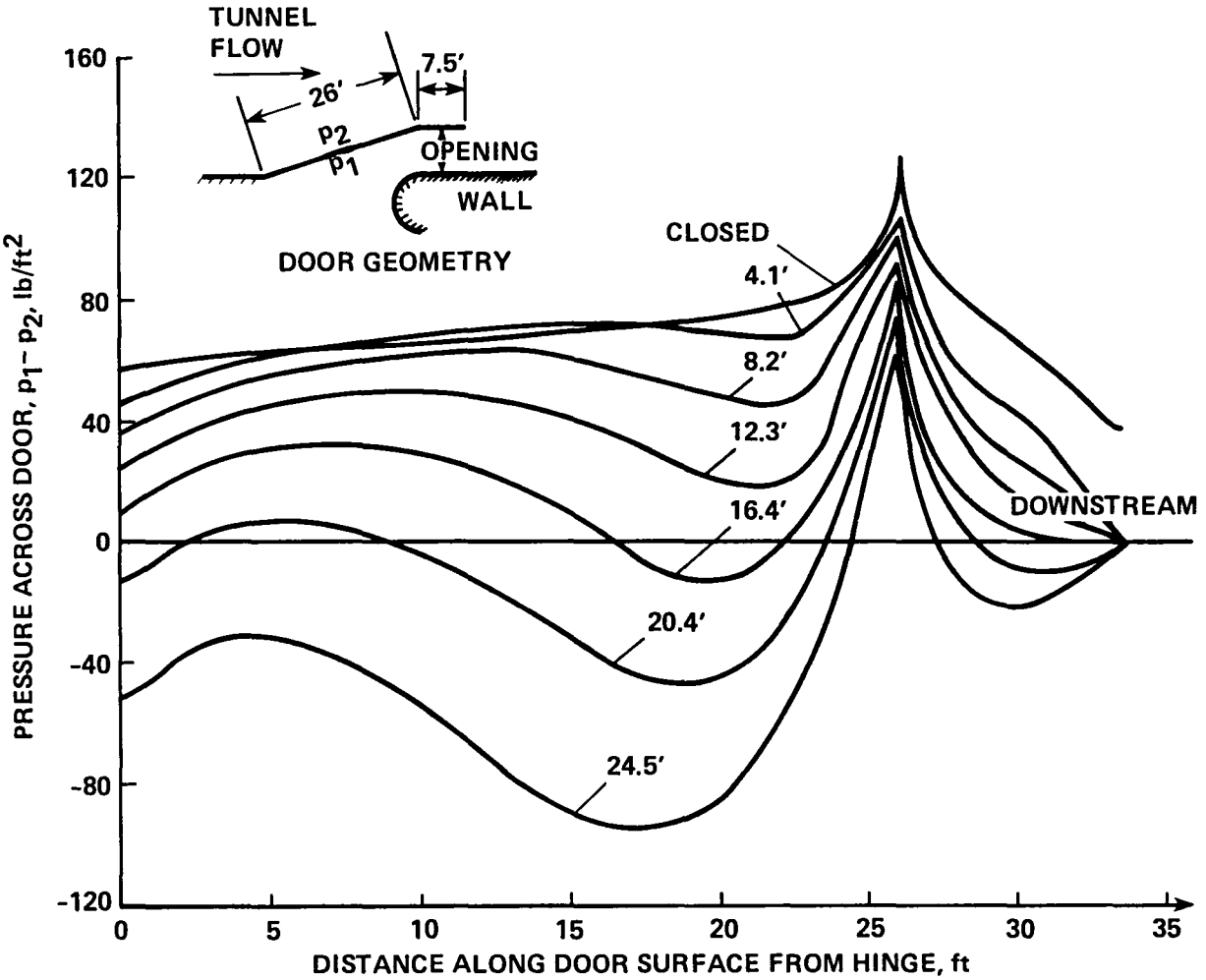

Figure 33.- Pressure differential across inlet door for several opening distances; p_n = -64 lb/ft^2.

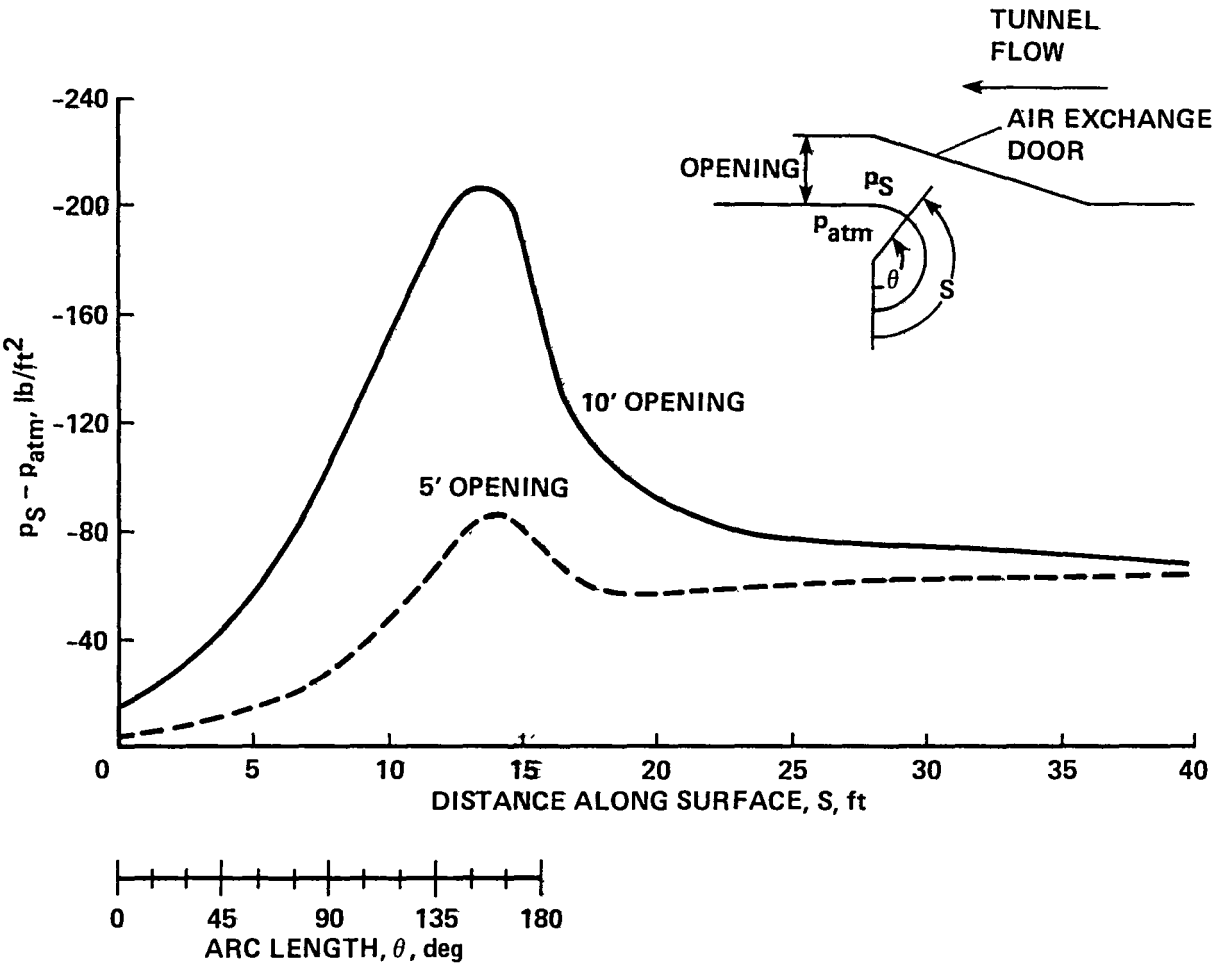

Figure 34.- Pressure on cowl and wall near inlet door opening as a function of distance along the surface when p_n = -64 lb/ft^2.

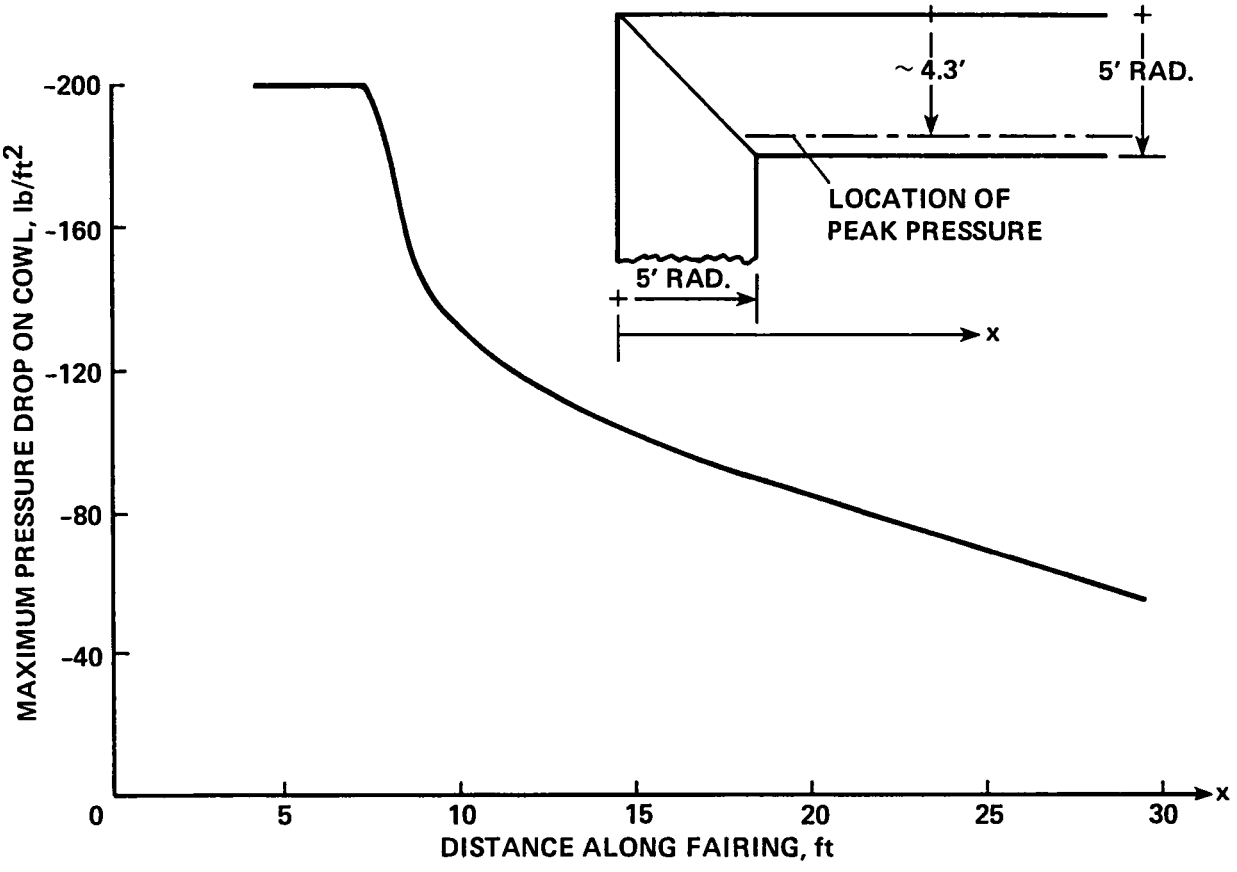

Figure 35.- Value of lowest pressure on horizontal cowl as a function of distance from outside edge of fairing when pressure in tunnel, p_n = -64 lb/ft^2. Pressure distributions on horizontal fairings are similar to those on vertical fairing but of decreasing magnitude as indicated above.

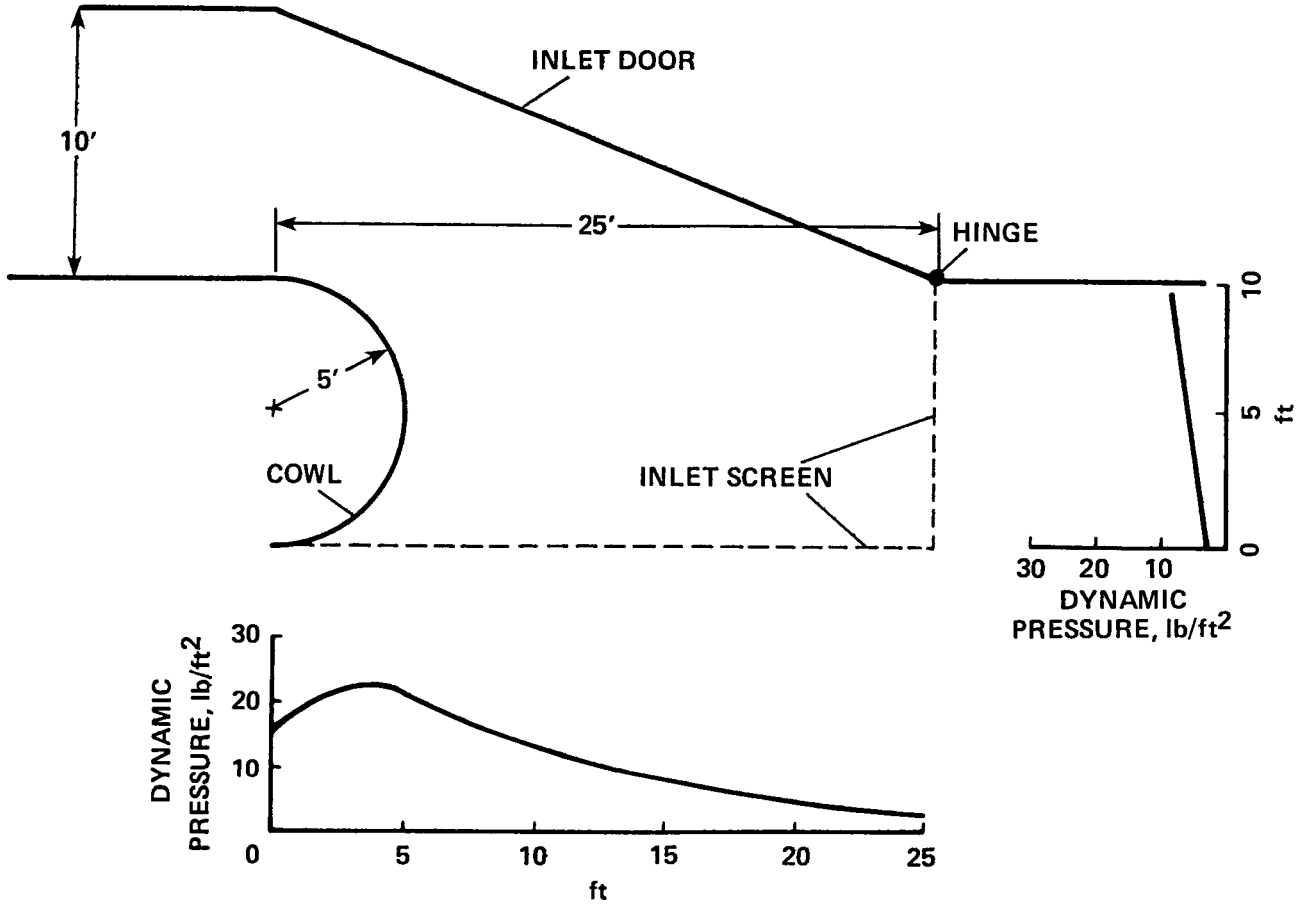

Figure 36.- Dynamic pressure distribution at location planned for debris screen which is to cover inlet, p_n = -64 lb/ft^2.

1 Report No	2 Government Accession No	3 Recipient's Catalog No
NASA TM-88192		

4 Title and Subtitle	5 Report Date
AERODYNAMIC CHARACTERISTICS OF AN AIR-EXCHANGER SYSTEM FOR THE 40- BY 80-FOOT WIND TUNNEL AT AMES RESEARCH CENTER	January 1986
	6 Performing Organization Code

7 Author(s)	8 Performing Organization Report No
Vernon J. Rossow, Gene I. Schmidt, Larry A. Meyn, Kimberley R. Ortner, Robert E. Holmes	A-86036
	10 Work Unit No

9 Performing Organization Name and Address	11 Contract or Grant No
Ames Research Center Moffett Field, CA 94035	

12 Sponsoring Agency Name and Address	13 Type of Report and Period Covered
National Aeronautics and Space Administration Washington, DC 20546	Technical Memorandum
	14 Sponsoring Agency Code 505-60-21

15 Supplementary Notes

Point of Contact: Vernon J. Rossow, Ames Research Center, MS 247-1, Moffett Field, CA 94035 (415) 694-6681 or FTS 464-6681

16 Abstract

A 1/50-scale model of the 40- by 80-Foot Wind Tunnel at Ames Research Center was used to study various air-exchange configurations. System components were tested throughout a range of parameters, and approximate analytical relationships were derived to explain the observed characteristics. It was found that the efficiency of the air exchanger could be increased (1) by adding a shaped wall to smoothly turn the incoming air downstream, (2) by changing to a contoured door at the inlet to control the flow rate, and (3) by increasing the size of the exhaust opening. The static pressures inside the circuit then remain within the design limits at the higher tunnel speeds if the air-exchange rate is about 5% or more. Since the model is much smaller than the full-scale facility, it was not possible to completely duplicate the tunnel, and it will be necessary to measure such characteristics as flow rate and tunnel pressures during implementation of the remodeled facility. The aerodynamic loads estimated for the inlet door and for nearby walls are also presented.

17 Key Words (Suggested by Author(s))	18 Distribution Statement
Wind tunnel design Air exchanger systems	Unlimited Subject category - 02

19 Security Classif (of this report)	20 Security Classif (of this page)	21 No of Pages	22 Price*
Unclassified	Unclassified	69	A04

*For sale by the National Technical Information Service, Springfield, Virginia 22161

End of Document